Calibration report for Avent 5-beam Demonstrator lidar

Borraccino, Antoine; Courtney, Michael

Publication date:
2016

Document Version
Publisher's PDF, also known as Version of record

UniTTe

Innovation Fund Denmark
RESEARCH, TECHNOLOGY & GROWTH

DTU

Calibration report for Avent 5-beam Demonstrator lidar

DTU Wind Energy E-Report-0087

A. Borraccino[1], M. Courtney[1]

DTU Wind Energy E-0087

March 2016

DTU Wind Energy
Department of Wind Energy

Author(s): A. Borraccino[1], M. Courtney[1]

Title: Calibration report for Avent 5-beam Demonstrator lidar

Department: DTU Wind Energy[1]

Abstract:
Nacelle-based profiling LiDARs may be the future of power performance assessment. Due to their large rotor size, single-point measurements are insufficient to quantify the power modern wind turbines can harness. The available energy in the wind indeed varies with heights. Improving power performance assessment by measuring simultaneously at different heights has been demonstrated using ground-based profiling LIDARs. Using nacelle lidars avoids the erection of expensive meteorology masts, especially offshore.

As for any other measuring system, lidars measurements have uncertainties. Their estimation is the ultimate goal of a calibration: a relation is established between reference measurements from calibrated instruments and corresponding LiDAR indications. Traceability in the calibration is obtained by transferring measurement uncertainties from the reference instrument through the calibration process.

A generic methodology to calibrate profiling nacelle lidars has been developed and performed on a 5-beam Demonstrator lidar manufactured by *Avent Lidar Technology*. In essence, the generic methodology calibrates the inputs of the wind reconstruction algorithms rather than their outputs.

This report presents the calibration procedures and results of a 5-beam Demonstrator unit. The calibration was performed at DTU's test site for large wind turbines, Høvsøre, Denmark. The methods to assess radial wind speed uncertainties are detailed together with an example of how to derive reconstructed wind parameters' uncertainties.

DTU Wind Energy E-0087

March 2016

ISBN: 978-87-93278-37-0

Contract no.: Innovationsfondens 1305-00024B

Project: UniTTe
http://www.unitte.dk/

Funding:
Innovation Fund Denmark

Pages: 83
Tables: 15
Figures: 37
References: 9

Technical University of Denmark
DTU Wind Energy
Risø Campus
Frederiksborgvej 399
DK-4000 Roskilde
Denmark

www.vindenergi.dtu.dk

Table of contents

Figures and tables

Nomenclature

a.g.l.: above ground level
CNR: carrier-to-noise ratio
CW: continuous wave
DK: Denmark
GPS: global positioning system
GUM: Guide to the expression of uncertainty in measurement [6]
HWS: horizontal wind speed
IEC: the International Electrotechnical Commission
LiDAR: light detection and Ranging
LOS: line-of-sight
R&D: Research and Development
RSS: residual sum of squares
RWS: radial wind speed
SI: International System of unis
SSR: sum of squares of residuals
VIM: International vocabulary of metrology [5]
WD: wind direction

α: cone or half-opening angle
α_{exp}: shear exponent of the assumed wind profile
β: effective half-opening angle
β_h: effective horizontal half-opening angle
β_v: effective vertical half-opening angle
ΔH_{pos}: height difference between lidar beam and reference instrument
ΔRWS: radial wind speed measurement error
θ: wind direction
θ_0: estimation of $\mathrm{LOS_{dir}}$
θ_{proj}: projection angle used to evaluate LOS_{dir}
φ_{BE}: best estimate of lidar tilt angle
$\varphi_{indicated}$: lidar indicated tilt angle
φ_{flow}: flow tilt angle
$\varphi_{physical}$: lidar's beam physical inclination
φ_{ref}: measured reference tilt angle
ψ_{BE}: best estimate of lidar roll angle
$\psi_{indicated}$: lidar indicated roll angle
ψ_{ref}: best estimate of lidar roll angle
$\langle\ \rangle$: scalar time average
$\langle\ \rangle_{\mathrm{vec}}$: vector time average
cov: covariance
$r(x, y)$: cross-correlation coefficient between x and y
σ_X: standard deviation of X

$D_{cal,X}$: calibration range for LOS X
$D_{physical}$: total distance between lidar and mast
D_{ref-0}: horizontal distance between reference lidar's point and the detected central beam position
f_{fit}: fitting function
H_0: height difference between the reference lidar's point and the detected central beam position
H_{mast}: height of meteorology mast a.g.l.
H_{lidar}: height of lidar a.g.l.
k: coverage factor
LOS_{dir}: LOS direction
L_X: (in tilt/roll calibration) horizontal distance number X
L_X: (other paragraphs) distance X
(N_X, E_X, Z_X): 3D coordinates of X measured with a total station
$Ref_{eq\ RWS}$: reference equivalent radial wind speed
R_{ij}: cross-correlation tensor between uncertainty components
RWS_{norm}: normalised radial wind speed
RWS_{BE}: best estimate of radial wind speed
$RWS_{indicated}$: lidar indicated radial wind speed
S_{hub}: lidar estimated horizontal wind speed at hub height
u_X: standard uncertainty of X
$u_{c,X}$: combined standard uncertainty of X
U_X: expanded uncertainty of X
u_φ: physical tilt inclination angle uncertainty
u_{cal}: calibration uncertainty of cup anemometer HWS
$U_{ext,X}$: extrapolated expanded uncertainty for LOS X
u_H: height uncertainty
u_{inc}: inclined beam uncertainty
$u_{LOS\ dir}$: LOS direction uncertainty
u_{mast}: mounting uncertainty of reference instrument on mast
u_{ope}: operational uncertainty of cup anemometer HWS
u_{pos}: positioning uncertainty
u_{range}: lidar measurement range uncertainty
u_{WD}: wind direction uncertainty
U: streamwise component of the horizontal wind speed vector
V: spanwise component of the horizontal wind speed vector
V_{rX}: radial or line-of-sight velocity of beam X

Preface

This document is the calibration report of an Avent 5-beam Demonstrator lidar. It has been written within work package 2 of the Unified Turbine Testing project (UniTTe, http://www.unitte.dk/) funded by *Innovation Fund Denmark*. UniTTe aims at developing power performance testing procedures using profiling nacelle-mounted lidars applicable in all types of terrain. Work package 2 focuses specifically on developing and performing calibration procedures to provide traceable lidars' measurements once installed on a turbine's nacelle.

One of the two lidars tested in UniTTe is a 5-beam pulsed system developed by *Avent lidar technology*. Its calibration was performed at DTU Wind Energy's test site for large wind turbines, Høvsøre, Denmark. The calibration procedures have been implemented following the *"Generic methodology for calibrating nacelle lidars"* described in deliverable D2.1 (DTU E-0086 report).

The calibration report is deliverable D2.2 and provides testing details specific to the Avent 5-beam Demonstrator lidar together with the calibration results and measurement uncertainties.

Antoine Borraccino
Ph.d.-student

Acknowledgements

I would first like to thank M. Courtney and R. Wagner who guided the work performed and reported in this document. This report really builds on M. Courtney's pioneering work on lidars' calibration and on the experience of the whole TEM section at DTU Wind Energy in calibrating ground-based, nacelle-based or even scanning lidars.

Thanks to M. Boquet and *Avent Lidar Technology* for supporting the UniTTe project and giving us the opportunity to test the 5-beam Demonstrator lidar. Thanks to S.A. Sørensen (DTU-TEM's database engineer) for answering all my database requests. Finally, a special thank you to DTU Wind Energy technicians A. Ramsing Vestergaard and K. Schrøder for imagining, designing and building all the necessary testing tools and for their expertise in lidars' beam detection while standing on top of a meteorology mast.

Chapter 1

1 Introduction

1.1 Profiling nacelle lidars in power performance testing

In recent years, the rapid increase in wind turbines size has created a need for developing new power performance assessment procedures. The effects of wind speed and direction variations over the rotor swept area on power curves can no longer be neglected [1]. Measuring the wind in one point, e.g. hub height, has consequently become insufficient.

LIght Detection And Ranging (lidar) is a remote sensing technology addressing this challenge. Its multiple applications have found their way into the wind energy market. Ground-based lidars are presently being used to measure wind profiles. They offer a practical and accurate solution for measuring wind over the entire rotor disk. On the other hand, even though two-beam nacelle lidars are unable to measure the wind shear, they show promising capabilities to assess power performance [2].

A wind profiling nacelle lidar measures the wind at multiple heights upstream of a turbine and from its nacelle – or downstream for wake measurements – thus eradicating the need for expensive meteorology masts, especially offshore. Additionally, nacelle lidars follow the turbine's movements. Consequently, in flat terrain or offshore, the exclusion of wind direction sectors for power performance analysis is limited to wakes from neighbouring turbines and is not required as often as with ground-based or floating lidars.

1.2 The Avent 5-beam Demonstrator lidar

1.2.1 Presentation

The 5-beam Demonstrator lidar (Figure 1) has been developed by *Avent Lidar Technology* for developing specific lidar-assisted turbine control projects with researchers and turbine manufacturers. In this section, the basic measurement principles and geometry of the 5-beam Demonstrator are presented.

Figure 1. The 5-beam Demonstrator on a 3 axis-rotating platform (left) and its tripod (right), Høvsøre, DK

1.2.2 Geometry and main measurement specifications

The 5-beam Demonstrator is a heterodyne pulsed Doppler system. It measures successively the wind along five line-of-sights (LOS), with a selectable measurement frequency of 1 or 4Hz (i.e. respectively 1 or 0.25 second / LOS). At each LOS measurement, up to 10 ranges are measured simultaneously (Figure 2).

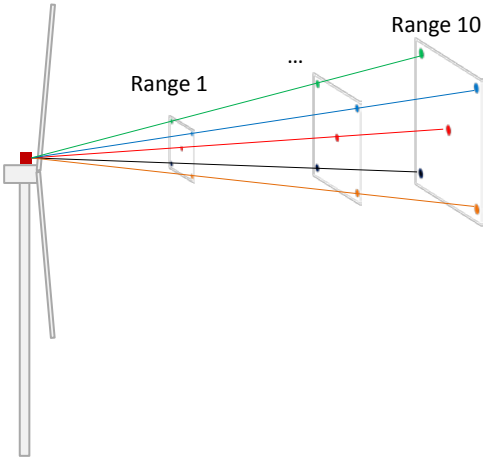

Figure 2. Schematic of the 5-beam lidar (Avent) mounted on the nacelle of a wind turbine

Two configurations are available: cross or square (see Figure 3). The pattern is pre-configured as it requires adjusting the position of internal parts (e.g. telescopes). In the UniTTe project, the square pattern has been chosen for the following reason: two beams are located at the lower and upper heights, allowing wind speed and direction reconstruction similarly to two-beam nacelle lidars at each of the heights.

For either configuration, when mounted on the nacelle and if there is no yaw misalignment, the radial wind speed (RWS) along LOS 0 is approximately the horizontal wind speed (HWS): $RWS0 \approx HWS$.

The cone angle – i.e. the angle between LOS0 and another LOS – is $\alpha = 15°$ (manufacturer specification). At the lower and upper heights, the effective half-opening angle between e.g. LOS1 and LOS2 is $\beta = \mathrm{atan}\left(\tan\alpha/\sqrt{2}\right) \approx 10.73°$.

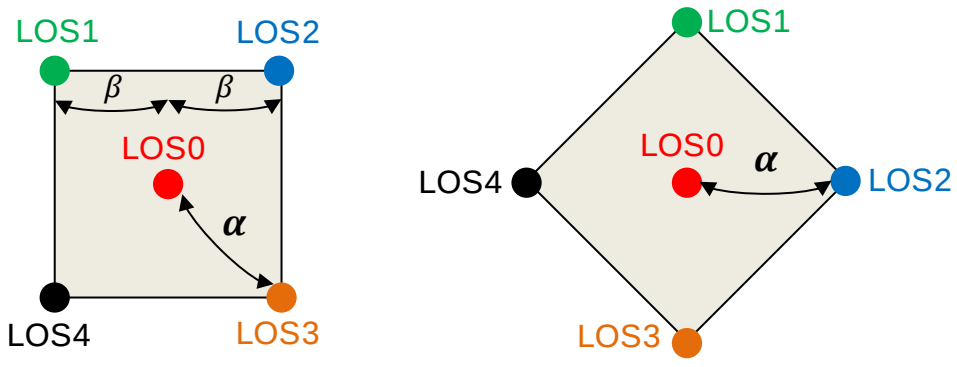

Figure 3. 5-beam lidar LOS geometry: square (left) and cross (right) configurations

As the 5-beam lidar is a pulsed system, its probe length depends mainly on the pulse duration and is constant with the measurement range. The effective pulse duration is estimated (lidar manufacturer) to $165\ ns$, corresponding to a probe length of $\left(\frac{165\ ns \cdot 3\times10^8}{2}\right) = 24.75m$, thus the minimum range is $\sim 50m$. The five telescopes focus the laser light at a fixed "vertical plane" distance of 125m, i.e. LOS0 is physically focused at 125m while LOS 1, 2, 3, 4 are focused at $125/\cos\alpha \approx 129.4m$. Depending on atmospheric conditions (e.g. aerosols concentration), the maximum range is approximately 300-350m. Greater ranges can be achieved by using a longer pulse duration, at the expense of poorer spatial resolution.

The five LOS use the same laser source and optical chain, except for the telescopes. In order to fulfil the formal requirements of an uncertainty calculation, each LOS should be calibrated. This is what has been performed in Høvsøre, one LOS after another. As the calibration of one LOS takes usually 3-6 weeks, the process is time-consuming and an alternative solution may be considered ([3], §.2.2.2). This alternative would be to calibrate a single randomly selected LOS and perform a study of the additional uncertainty due to the adjustment of each telescope (CNR and focus). This extra uncertainty is likely to be negligible compared to the reference instrument uncertainties.

1.2.3 Recorded measurement data

The 5-beam Demonstrator provides both 10-minute statistics and, every second, one RWS measurement on successive LOSs (referred to as fast or realtime data). Three levels of data can be distinguished, i.e. raw data (RWS, beam positions, availability), local reconstructed parameters (wind characteristics estimated at each range) and global reconstructed parameters (wind characteristics estimated using measurements at several ranges and a 3D wind field model):

- **Realtime**
  - Raw measurements: timestamp, RWS, Carrier-to-Noise Ratio (CNR), tilt and roll inclination angles.
  - Local reconstructed parameters: HWS, horizontal and vertical shears.
  - Global reconstructed parameters: HWS, longitudinal, horizontal and vertical shears, relative wind direction (i.e. yaw misalignment), flow angle (also called vertical wind direction).
- **10-min statistics:**
  - Raw measurements (along each LOS and at each range): averages of relatime data and LOS availability.
  - Local reconstructed parameters: averages of realtime data and parameters availability.
  - Global reconstructed parameters: averages of realtime data and parameters availability.

For the RWS calibration, only the 10-minute statistics of the raw measurements are used.

1.3 Choice of calibration method

The 5-beam Demonstrator calibration was performed using the "white box methodology" detailed in [3]. The white box approach consists in calibrating the input quantities of the lidar's reconstruction algorithms rather than calibrating each reconstructed wind parameter – referred to as the black box methodology.

For the 5-beam Demonstrator, these inputs are the geometry of the lidar's beams pattern, – i.e. opening angles between the lidar centreline and the LOS – the tilt and roll inclinometers measurements and the RWS velocity along each LOS.

1.4 Timeline of events

The 5-beam Demonstrator lidar has been calibrated at DTU Wind Energy's test site for large wind turbines between November 2014 and April 2015. The timeline of the main events is (time synchronisation to GMT+1):

- **Inclinometers calibration** (tilt and roll) and **geometry verification** – *2014-10-29* and *2014-10-30*
- Individual LOS calibration order:

  LOS 0 (part 1) – LOS 4 – LOS 1 – LOS 0 (part 2) – LOS 3 – LOS 2
- Lidar installation (see Figure 15) on *2014-10-31 10:00*
- **LOS 0 calibration**

  (Part 1)
  - Theodolite measurements, hard target tests, beam positioning, ranges configuration at *2014-10-31 10:00*
  - Valid measurement period: *[2014-10-31 14:00 ; 2014-12-10 08:30]*
  - Lidar stopped *[2014-11-14 13:41:29 ; 2014-11-24 15:04:49]* for laser-safety checks
  - Beam position check before moving at *2014-12-10 08:50*

  (Part 2)
  - Re-positioning, switching from LOS 1 to LOS 0, at *2015-02-05 12:00*
  - Valid measurement period: *[2015-02-05 15:30 ; 2015-02-23 10:00]*
  - Beam position check before moving at *2015-02-23 10:20*
- **LOS 4 calibration**
  - Re-positioning, switching from LOS 0 to LOS 4, at *2014-12-10 09:20*
  - Valid measurement period: *[2014-12-10 10:20 ; 2015-01-06 09:20]*
  - Beam position check before moving at *2015-01-06 09:40*
- **LOS 1 calibration**
  - Re-positioning, switching from LOS 4 to LOS 1, at *2015-01-06 10:10*
  - Valid measurement period: *[2015-01-06 10:50 ; 2015-02-05 11:20]*
  - Beam position check before moving at *2015-02-05 11:30*
- **LOS 3 calibration**
  - Re-positioning, switching from LOS 0 to LOS 3, at *2015-02-23 11:20*
  - Valid measurement period: *[2015-02-23 12:40 ; 2015-03-19 09:40]*
  - Beam position check before moving at *2015-03-19 10:00*
- **LOS 2 calibration**
  - Re-positioning, switching from LOS 3 to LOS 2, at *2015-03-19 10:30*
  - Valid measurement period: *[2015-03-19 12:00 ; 2015-04-20 12:00]*
  - Beam position check at *2015-04-20 12:20*

Chapter 2

2 Inclinometers calibration and geometry verification

This section concerns the calibration of the tilt and roll inclinometers of the Avent 5-beam Demonstrator. The procedure is adapted from the two-beam nacelle lidars's procedure and described in [4]. The section also provides the geometry verification since it is performed with a similar measurement setup.

2.1 Principles

The internal inclinometers are calibrated by comparing the lidar tilt and roll readings with reference quantity values obtained by: detecting the beams' positions; measuring the 3D positions of the beams and of a reference point on the lidar close to the beam origin. In practice, we are only interested in the height difference and horizontal distance between the beam position and the origin of the beams.

2.1.1 Defining the zeros axes of inclination

The zero axes of inclination are defined (by us, the calibration institute) as[1]:

- 0° tilt when LOS 0, i.e. the lidar optical centreline, is horizontal.
- 0° roll corresponds to LOS 3 and 4 (bottom pair[2]) being located at the same height relatively to a horizontal plane passing through the origin of the beams.

2.1.2 Measurement setup

In the calibration, the transfer functions between the indicated tilt and roll and the actual measured values, with respect to the above definitions, are derived. The measurement setup (Figure 4) is composed of:

- The 5-beam Demonstrator lidar
- One central frame, mainly used during the tilt calibration and geometry verification, ~4m high.
- Two side frames for the roll calibration and geometry verification, ~3m high.
- Shutters on each frame, which positions can be adjusted in two directions.
- One range-finding theodolite ('total station'), providing 3D coordinates (N, E, Z) measurements (see Figure 5). The theodolite is levelled, thus the Z coordinate is in a vertical axis. The axis N and E are orthogonal and define a horizontal plane passing through the origin of the theodolite reference frame.
- One computer connected to the lidar for live observations, e.g. of CNR responses.

[1] We, at DTU Wind Energy, who performed the testing, arbitrarily chose these definitions. Note that the tilt inclinometer zero corresponds to the manufacturer's definition (*Avent Lidar Technology*).
[2] Note that the top pair (LOS 1 and 2) may also have been used.

Figure 4. Left: photograph of the measurement setup for ground calibration of the 5-beam Demonstrator's inclimometers. Right: shutters for detecting the beam position by blocking/unblocking

Figure 5. 3D coordinates measurements with a theodolite

Figure 6 shows additional details on the measurement setup:

- The distance between the lidar and the frame should be as large as possible to minimise the uncertainty in the tilt and roll angle measurements. The measurement distance is however limited by the range of tilt angles to calibrate and by the height of the frames. Here the distance was ~30m, giving a tilt angle range of approximately ±2°.
- The position of the theodolite has little importance. An adequate position ensures that all the points of interest are measurable (without moving the theodolite) and that the theodolite never blocks the lidar's beams. Typically, it can be placed approximately halfway between the lidar and the frames, and halfway between the central frame and one side frame.
  Note: from the point of view of eye-safety, it is important that the theodolite is placed in an area where it cannot come into contact with any of the lidar beams, as the magnifying effect of the theodolite lens could cause eye safety issues.

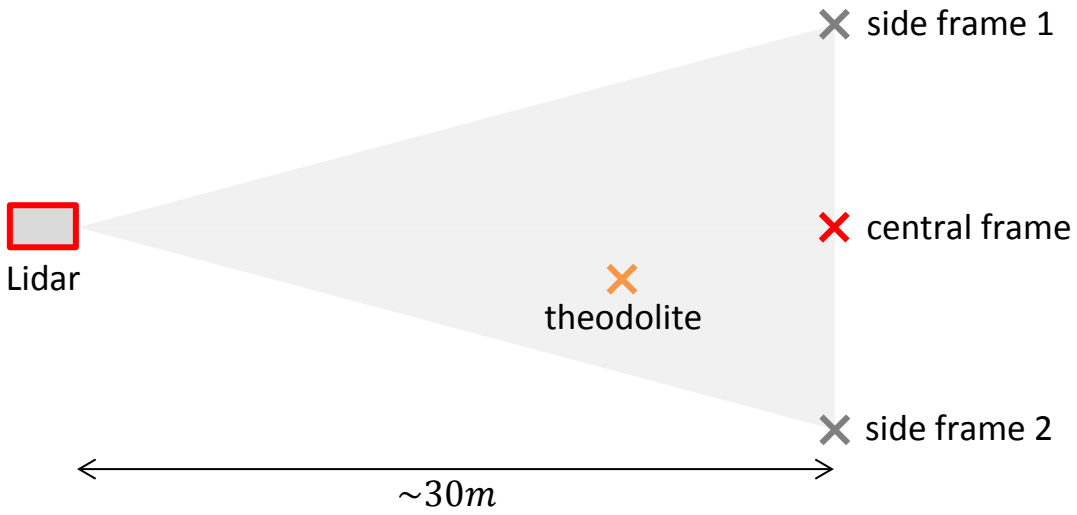

Figure 6. Top-view schematic of the measurement setup for inclinometers calibration

2.1.3 Accurately detecting the beam position

The beam position is detected by an iterative process of blocking and unblocking until the beam passes through a narrow area defined by the shutters (see Figure 7).

The lidar is configured with measurement ranges distinct from each other: e.g. 50m, 75m, 100m, 150m, 200m. When one beam hits a hard target such as the shutters, its CNR signal drops massively at ranges greater than the physical distance between the lidar and the frame. Indeed, the lidar is "blinded" at greater distances. If a range close to the physical distance is configured, the CNR should show a peak at that specific distance due to high backscatter (see Figure 7).

Once the shutters have been maneuvered to contain the beam, the position of a black cross on the shutter (Figure 4), having a known offset to the shutter centre, is measured from the theodolite. In this way, the lidar beam position is measured with an estimated uncertainty of $10\ mm$, of the same order of magnitude as the beam diameter.

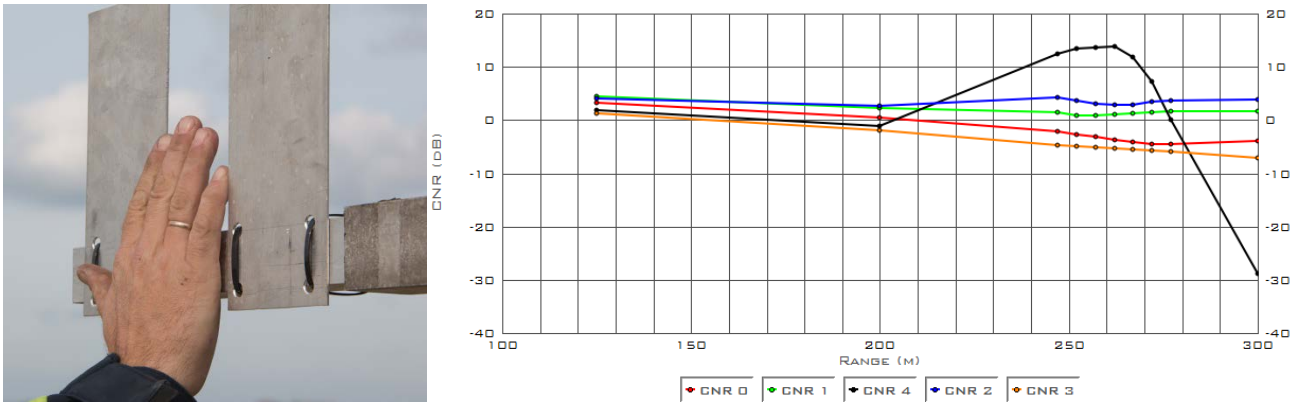

Figure 7. Shutters (left) and CNR response (right) of a pulsed lidar hitting a hard target at 255m: example of the 5-beam Demonstrator lidar (Avent).

2.2 Optical head geometry and origin of the beams

The origin of the lidar's beam can be considered with good approximation to be at the center of the lidar's window on the optical head (point B0, see Figure 8). Practically, two points are marked (crosses C2 and C3) on the optical head and measured for each tilt and roll configuration. The full geometry of optical head's windows is measured once, allowing to reconstruct the coordinates $(N_{ref}, E_{ref}, Z_{ref})$ of its center.

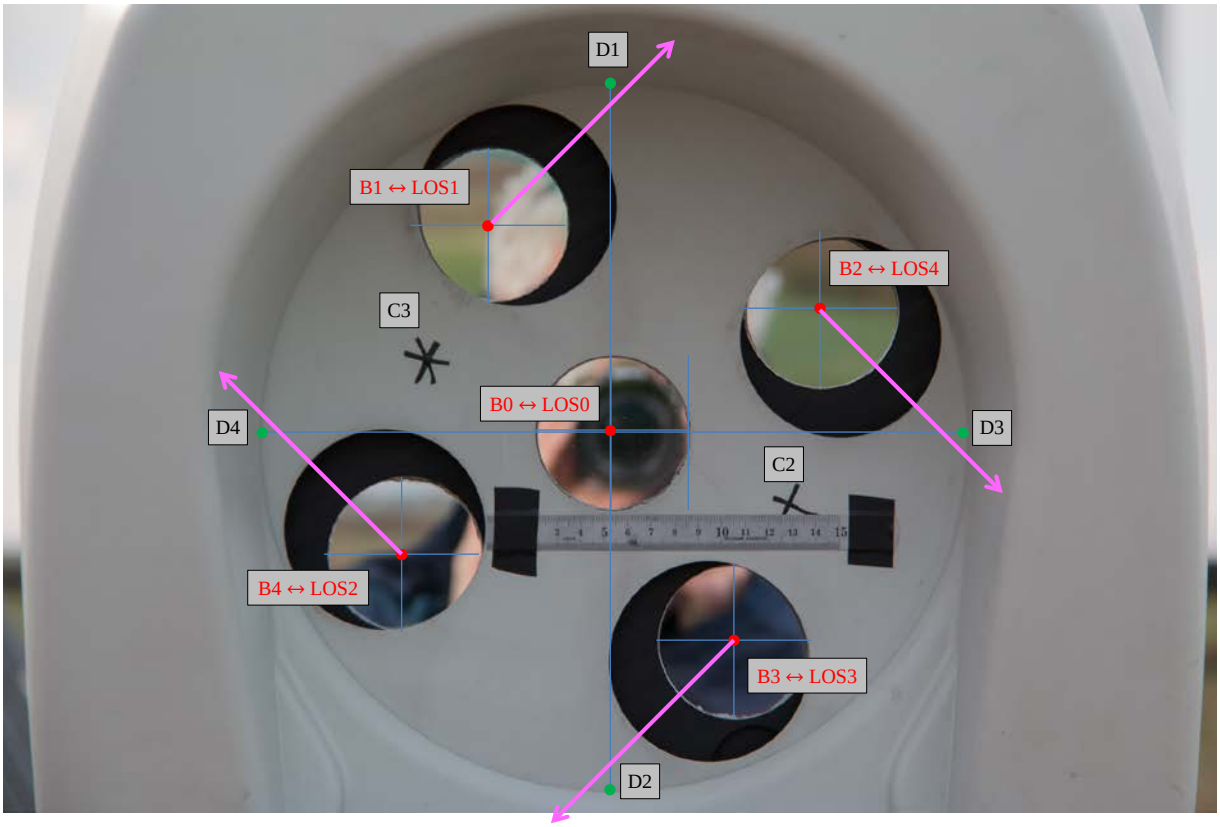

Figure 8. Geometry of the lidar's optical head windows

2.3 Tilt calibration

2.3.1 Procedure

The tilt calibration is performed by successively placing the lidar in different tilting positions, at $\sim 0°$ roll. For each tilt position:

- the following theodolite measurements (N, E, Z) are taken:
  - position of LOS 0 (N_0, E_0, Z_0), using the central frame.
  - position of the two reference points (C2 and C3, see Figure 8) on the optical head
- the coordinates of the center of the lidar's windows are derived: $(N_{ref}, E_{ref}, Z_{ref})$.

The process is repeated typically 8-10 times for tilt angles in the $\pm 2 - 3°$ range, corresponding to typical operational conditions of a nacelle lidar.

2.3.2 Geometrical development

Figure 9 shows a schematic and a photograph of the tilt calibration setup. The measured tilt angle φ_{ref}, i.e the reference quantity value, is given by:

$$\varphi_{ref} = \text{atan}\left(\frac{H_0}{D_{ref-0}}\right) \quad \text{(eq. 1)}$$

where the height difference $H_0 = Z_0 - Z_{ref}$ and the horizontal distance between the detected position of LOS 0 is $D_{ref-0} = \sqrt{\left(N_0 - N_{ref}\right)^2 + \left(E_0 - E_{ref}\right)^2}$.

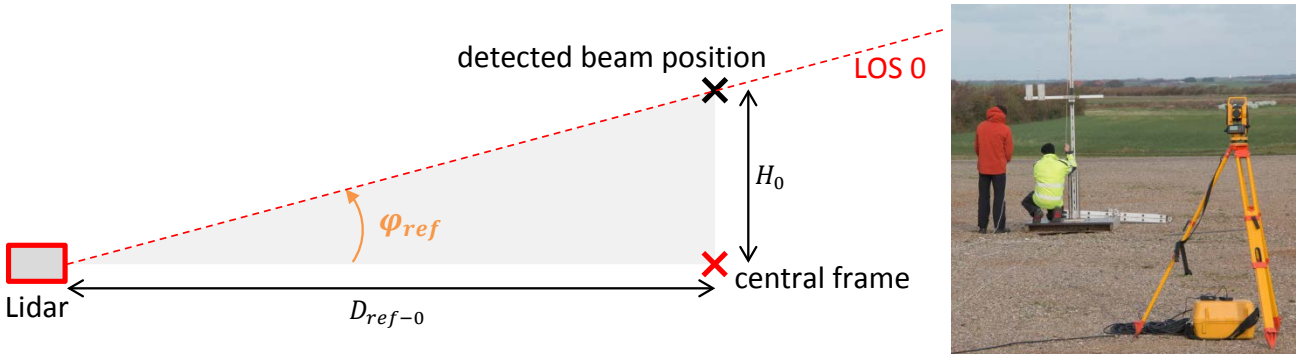

Figure 9. Side-view schematic of the tilt calibration (left). Photograph of the measurement setup (right)

2.3.3 Results

The tilt calibration results are presented in Figure 10. The retained calibration relation is the unforced linear regression:

$$\varphi_{BE} = 1.0123 \cdot \varphi_{indicated} + 0.0471$$

where φ_{BE} is the best estimate of the tilt angle, i.e. the calibrated tilt angle obtained by correcting the lidar indicated tilt $\varphi_{indicated}$. The calibration is incomplete if the measurement uncertainty is not specified (cf. metrological definition in [5]). The tilt calibration uncertainties are derived using the GUM methodology (see [6]) and detailed in Annex B. u_{H_0} being the uncertainty of the measured height difference H_0, the tilt angle uncertainty in radians is simply: $u_{c,\varphi_{ref}} = u_{H_0}/D_{ref-0}$. The expanded uncertainty on φ_{BE} with a coverage factor of 2 is: $U_{\varphi_{BE}} = 0.05°$.

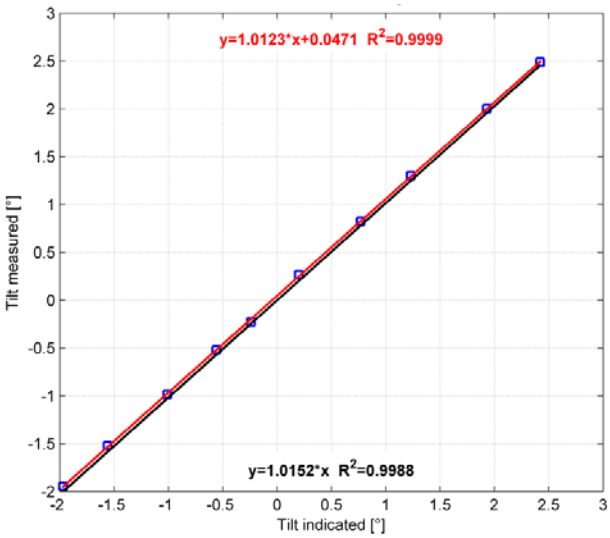

Figure 10. Tilt calibration results: measured vs. lidar indicated

2.4 Roll calibration

2.4.1 Procedure

The roll calibration is performed by successively placing the lidar in different rolling positions, at $\sim -10.73°$ tilt so that the bottom pair (LOS 3 and 4) is close to horizontal. For each roll position:

- the following theodolite measurements (N, E, Z) are taken:
  - position of LOS 3 (N_3, E_3, Z_3), using side frame #2 (Figure 6)
  - position of LOS 4 (N_4, E_4, Z_4), using side frame #1
  - position of the two reference points (C2 and C3, see Figure 8) on the optical head
- the coordinates of the center of the lidar's windows are derived: $(N_{ref}, E_{ref}, Z_{ref})$.

The process is repeated 8-10 times for roll angles between $\pm 5°$.

2.4.2 Geometrical development

The geometrical development to derive the measured roll angle is similar to the method detailed in [4]. Figure 11 illustrates the roll calibration setup. The lidar is at point A, LOS 3 and LOS 4 are detected respectively at C' and B'.

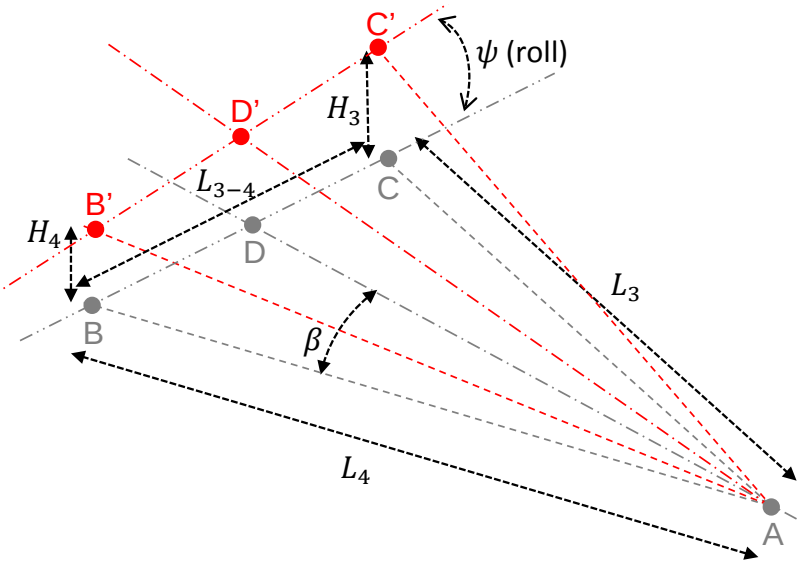

Figure 11. Schematic of the roll calibration measurement setup

Using the theodolite measurements, one can derive:

- Height differences: $H_3 = Z_3 - Z_{ref}$ and H_4 alike.
- Horizontal distances:
  - $L_3 = \sqrt{\left(N_3 - N_{ref}\right)^2 + \left(E_3 - E_{ref}\right)^2}$ and L_4 alike.
  - $L_{34} = \sqrt{(N_4 - N_3)^2 + (E_4 - E_3)^2}$
- The experimental half-opening angle β is the half-opening angle between LOS 3 and 4 as defined in Figure 3 (left). The law of cosines gives:

$$\beta = \operatorname{acos}\left(\frac{L_3^2 + L_4^2 - L_{34}^2}{2L_3L_4}\right) \quad \text{(eq. 2)}$$

- The roll angle is finally given by:

$$\psi = \operatorname{atan}\left(\frac{\frac{H_3}{L_3} - \frac{H_4}{L_4}}{2 \cdot \sin\beta}\right) \quad \text{(eq. 3)}$$

2.4.3 Results

The roll calibration results are presented in Figure 12. The retained calibration relation is the unforced linear regression:

$$\psi_{BE} = 1.0062 \cdot \psi_{indicated} - 0.0864\ [°]$$

where ψ_{BE} is the best estimate of the roll angle, i.e. the calibrated roll angle obtained by correcting the lidar indicated roll $\psi_{indicated}$.

The roll calibration uncertainties are derived similarly to the tilt calibration and detailed in Annex B. The uncertainty on ψ_{BE} with a coverage factor of 2 is: $U_{\psi_{BE}} = 0.18°$.

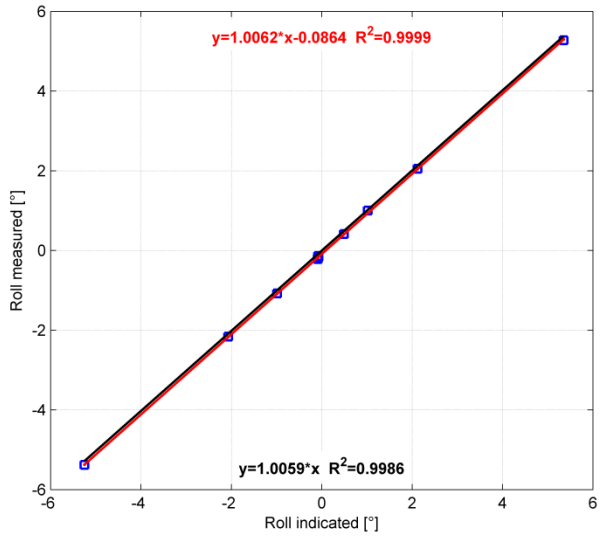

Figure 12. Roll calibration results: measured vs. lidar indicated (left). Photograph of the 5-beam Demonstrator lidar during the roll calibration, Høvsøre, DK (right).

2.5 Geometry verification

2.5.1 Procedure

The geometry verification is performed by rolling the lidar by approximately $\pm 45°$ using a spirit level, and at $\sim 0°$ tilt. Thus, three beams are forming a next-to-horizontal line: LOS 1-0-3 corresponds to the $+45°$ configuration, and LOS 4-0-2 to $-45°$ (see Figure 13).

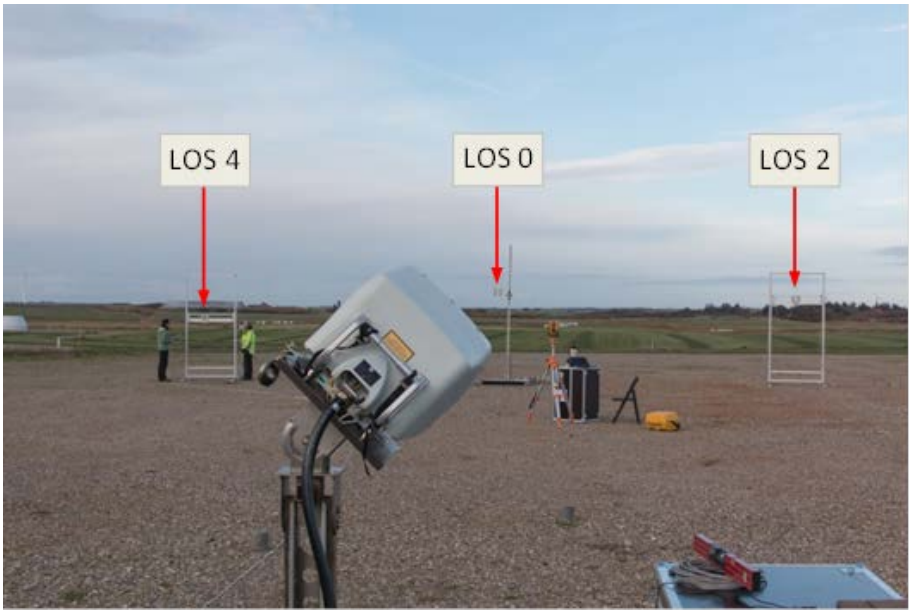

Figure 13. Photograph of the measurement setup for geometry verification of the 5-beam Demonstrator

At $-45°$ roll:

- the following theodolite measurements are then taken:
  - position of LOS 4 (N_4, E_4, Z_4), using the side frame #1
  - position of LOS 2 (N_2, E_2, Z_2), using the side frame #2
  - position of LOS 0 (N_0, E_0, Z_0), using the central frame
  - position of the two reference points on the optical head
- the coordinates of the center of the lidar's windows are derived: ($N_{ref}, E_{ref}, Z_{ref}$).

At $+45°$, the measurements are the same, substituting LOS4 and LOS2 by LOS 1 and LOS 3 respectively. Finally, the process is repeated 3-4 times at slightly different tilt angles, e.g. between $\pm 1°$, to verify the obtained values of the opening angles.

2.5.2 Geometrical development

The measured half-opening – or cone – angles are the opening angles between each corner beam and LOS 0. It is derived using the same method as in 2.4.2. ($X = 1, 2, 3$ or 4):

- Horizontal distances are derived between:
  - the lidar and LOS X: $L_X = \sqrt{\left(N_X - N_{ref}\right)^2 + \left(E_X - E_{ref}\right)^2}$.
  - the lidar and LOS 0: $L_0 = \sqrt{\left(N_0 - N_{ref}\right)^2 + \left(E_0 - E_{ref}\right)^2}$
  - LOS 0 and LOS X: $L_{0X} = \sqrt{(N_0 - N_X)^2 + (E_0 - E_X)^2}$.

- The experimental cone angle α_X is given by:

$$\alpha_X = \operatorname{acos}\left(\frac{L_X^2 + L_0^2 - L_{0X}^2}{2L_0L_X}\right) \quad \text{(eq. 4)}$$

2.5.3 Results

Table 1. Geometry verification of the 5-beam Demonstrator lidar: measurement of opening angles

$\alpha_{LOS0-LOS1}$	$\alpha_{LOS0-LOS2}$	$\alpha_{LOS0-LOS3}$	$\alpha_{LOS0-LOS4}$
$\mathbf{15.07°}$	$15.09°$	$15.11°$	$15.06°$

The geometry verification results are presented in the table above. Due to the design of the 5-beam Demonstrator (internal positions of the telescopes), the opening angles are expected to be slightly larger than $15°$ at short range. For information, at a $50m$ distance – close to the measurement setup – the expected value is $\alpha_{th} = 15.04°$, which is consistent with the verification results obtained at 30m.

Chapter 3

3 RWS calibration

This section describes the measurement setup of the RWS calibration of the 5-beam Demonstrator lidar and provides the calibration results for each of the five LOSs.

3.1 Measurement setup

3.1.1 Measurement systems

The measurement setup providing the required data of the RWS calibration campaign is:

- Reference instruments (Figure 14):
  - top-mounted on two met. masts laterally (with reference to the beam) separated by $5.3m$ at a height a.g.l. $H_{mast} = 8.9m$.
  - one cup anemometer: to measure horizontal wind speed, type Thies First class advanced (see calibration certificate in Annex C and classification in [7]).
  - one sonic anemometer: to measure wind direction, type Gill 1210R3-50 (see calibration certificate in Annex D).

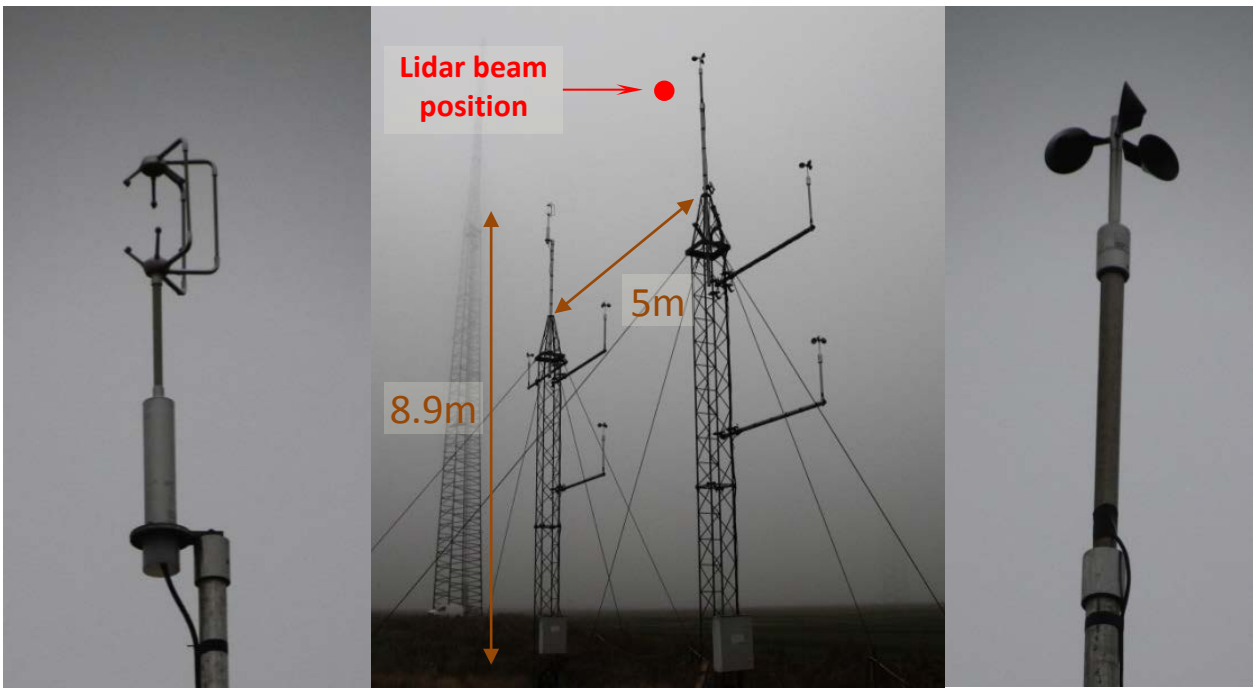

Figure 14. Reference instruments for RWS calibration: sonic anemometer (left), two masts (center), cup anemometer (right)

- 5-beam Demonstrator mounted on a 3-axis rotating platform (Annex A) and placed on stable ground (see Figure 15)
    - ~262m from the reference instruments. The terrain between the lidar and the masts is a flat open field.
    - the tilting is adjusted until the beam is located close to the reference instruments. The resulting physical[3] tilting is identical for each of the 5 beams[4]:

$$\varphi_{physical} = \text{atan}\left(\frac{H_{mast} - H_{lidar}}{D_{physical}}\right) \approx 1.6° \qquad \text{(eq. 5)}$$

Figure 15. Calibration measurement setup of the Avent 5-beam Demonstrator lidar at DTU Wind Energy test site, Høvsøre (DK)

3.1.2 Range configuration

The distance between the lidar and the cup anemometer – i.e. the main reference instrument – has been measured to $D_{cal} = 262.1m$ using the theodolite. The lidar measurement range is defined along LOS 0. Thus, the measurement range for the calibration is: $D_{cal,0} = 262m$ for LOS0; $D_{cal,X} = 253m$ for the other four LOS ($262 \cdot \cos 15°$).

The following range configuration was used for all LOS:

$$[125m\,;\ 247m\,;\ 252m\,;\ 257m\,;\ \mathbf{262m}\,;\ 267m\,;\ 272m\,;\ 277m\,;\ 282m\,;\ 300m]$$

In this configuration, ranges are centered on the measurement distance of 262m and regularly spaced. Two measurement ranges are taken further away (125m and 300m) from the reference instruments. The chosen range configuration allows sanity checks on the lidar sensed range using statistical methods (see 3.5.2).

Note: during the Høvsøre campaign, the range configuration remained centered at 262m for all LOS calibrations. For best practices in future campaigns, this will be changed to be centered on 253m for LOS 1, 2, 3 and 4. The 252m distance was used for the calibration of LOS 1, 2, 3 and 4.

[3] Physical as opposed to the lidar reading of the tilt inclination, based on LOS 0.

[4] The inclinometers read $\sim -9.1°$ and $\sim +12.3°$ respectively when one of the upper (LOS 1 & 2) or lower (LOS 3 & 4) beams is being calibrated. The physical tilting of the beam being calibrated however remains the same (~1.6°).

3.1.3 Reasons for choosing the Høvsøre measurement setup

The two met. masts were initially installed for previous research projects. Developing the procedures and performing calibrations using reference instruments mounted on these masts was convenient. Even though the measurement setup is certainly not optimal, they are suitable for the RWS calibration of nacelle lidars and provide the necessary data. The reasons for using the described measurement setup (3.1) are:

- Site location and characteristics: Høvsøre is located on the West coast of Jutland in Denmark, ~2km from the sea and the terrain is flat.

- Wind climate: strong westernly winds coming from the North Sea are typical (Annex F). Consequently, the calibration can be completed faster since filling in high wind speed bins is usually the most time-consuming part of the calibration.

- Height of the two met. masts: nacelle lidars should be calibrated in conditions similar to the operational ones. However, measuring at typical modern wind turbines' hub height (~ 80-100m) is in practice difficult. The lidar would need to be placed on a stiff platform to avoid measurement uncertainties due to the tilting and rolling of the structure (see [4]). At such heights, stiff structures (e.g. concrete) are extremely expensive. Thus, the height of 10m was preferred and more suitable since the lidars could, at first, be placed on a 10m platform in a mast, so that the beam is horizontal while being calibrated. Placing the lidar on the ground with its beam tilted up is a valid alternative, as demonstrated in [3] and this report. On the negative side, the 10m height a.g.l. implies relatively high turbulence which is known to impact reference anemometers (e.g. cups). Consequently, the ideal setup would have to compromise between measuring at greater heights and limiting the tilting of the beam.

- Measurement distance: one of the main applications of profiling nacelle lidars is the measurement of power curves. Standards in power performance ([8]) currently require the wind to be measured at distances equivalent to 2.5 rotor diameters – i.e. 250-300m for modern wind turbines. The measurement distance of ~260m in the calibration setup fits well these requirements. Additionally, it allows testing nacelle lidars close to the limits of their current measurement range capabilities.

- Reference instruments: for decades, the wind industry mainly relied on cup anemometers and wind vanes for wind speed and direction measurement. Current standards specify ([8]) how to assess the uncertainty of cup anemometers. Sonic anemometers seem like a viable alternative although their operational measurement uncertainty is not yet thoroughly implemented in standards. We chose to rely on two reference instruments – one cup anemometer for wind speed (main driver of (eq. 10)), and one sonic for wind direction – rather than only a sonic anemometer. Both are affordable instruments.

- Two masts or one? Both reference instruments are top-mounted on their respective mast in order to prevent mutual flow perturbation, and to minimise mounting uncertainties. However, one could also consider using only one mast and alternative mounting techniques allowing the two instruments to measure at the same height.

3.2 Beam positioning technique

The employed positioning technique makes use of a hard target, similarly to 2.1.3. The difference lies in the use of a simple stick, with a reflective surface at its extremity, rather than shutters. The length L_{stick} and angle γ from the mast to the stick are adjusted until the beam is known to hit the extremity of the stick, and both are then measured (see Figure 16). The distance L_{cup} from the attachment point to the cup anemometer is also measured. The height difference ΔH_{pos} between the beam position and the top-mounted cup anemometer is then obtained:

$$\Delta H_{pos} = L_{stick} \cdot \cos\gamma - L_{cup} \quad \text{(eq. 6)}$$

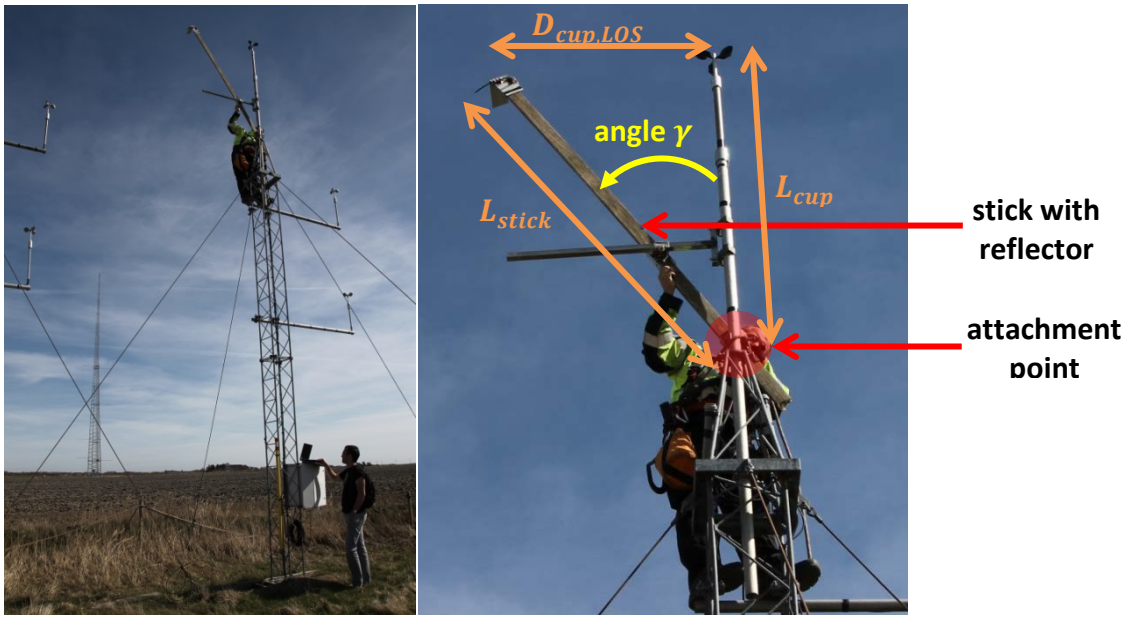

Figure 16. Positioning the beam close to the reference anemometer

If the height difference ΔH_{pos} is found to be unacceptably large, the lidar tilt is adjusted and the aforementioned steps repeated. This procedure allows to accurately position the beam close to the reference anemometer. Typically, ΔH_{pos} is within ± 5 cm and the beam is positioned ~1-2m laterally away from the cup anemometer. To be conservative, the beam height uncertainty is estimated to $u_H = 10cm$ (see 4.1.1). Table 2 provides results of beam position measurements, including the horizontal distance to the cup anemometer $D_{cup,LOS}$, before the calibration ("setup") and once it is complete ("check before moving").

Table 2. Beam position measurements before and after data collection

	Height difference Δhpos (cm)		Horizontal distance to cup (cm)	
	setup	check before moving	setup	check before moving
LOS 0 (part 1)	7,5	6,1	97,3	90,4
LOS 4	-4,8	-1,2	80,1	81,3
LOS 1	-0,8	-2,3	88,7	91,4
LOS 0 (part 2)	not measured	-6,0	not measured	182,2
LOS 3	0,5	-8,1	151,1	145,7
LOS 2	-0,8	-3,5	115,0	117,5

3.3 Data analysis

3.3.1 List of data

The list of data used in the analysis and filters is given in Table 3. Note: the data listed below are based on 10-minute statistics.

Table 3. List of data for RWS calibration analysis

Symbol	Unit	Description (instrument)
$\langle HWS \rangle_{vec}$ or $\langle HWS \rangle_{vec,\ cup}$	m/s	Vector mean horizontal wind speed (cup anemometer)
$\langle \varphi_{ind} \rangle$	deg	Lidar tilt angle indication (lidar)
$\langle \varphi_{BE} \rangle$	deg	Best estimate of lidar tilt angle corrected using the tilt calibration results
$\langle \varphi_{phys} \rangle$	deg	Physical lidar tilt angle (10-min averages): - For LOS 0, $\langle \varphi_{phys} \rangle = \langle \varphi_{BE} \rangle$ - For LOS 1 and 2, $\langle \varphi_{phys} \rangle = \langle \varphi_{BE} \rangle + \beta$, where $\beta = 10.73°$ (see Figure 3) - For LOS 3 and 4, $\langle \varphi_{phys} \rangle = \langle \varphi_{BE} \rangle - \beta$
$\langle \theta \rangle_{vec}$	deg	Vector mean horizontal wind direction (sonic anemometer)
$\langle HWS \rangle_{vec,\ sonic}$	m/s	Vector mean horizontal wind speed (sonic anemometer)
$\langle \varphi_{flow} \rangle$	deg	Flow tilt angle (sonic anemometer)
$\langle CNR \rangle$	dB	Carrier-to-noise ratio (lidar)
LOS_{avail}	%	LOS availability (lidar) $LOS_{avail} = \frac{number\ of\ valid\ data\ points}{maximum\ number\ of\ points\ in\ 10min}$
LOS_{count}	-	Number of attempts to measure one LOS velocity.
$StatA_{sonic}$	-	The status address is a binary result message, generated at the sonic sampling frequency (i.e. 20 Hz)

3.3.2 Filters

The valid dataset of 10-min averaged data is obtained by filtering as follows, except for the LOS direction estimation using the fitting technique (3.3.3.1) for which the wind direction filter is not applied:

- Vector mean HWS from cup anemometer:
  - $\langle HWS \rangle_{vec} \in [4\ ;\ 16]\ m.s^{-1}$
  - corresponding to the calibrated range of HWS.
- Check of HWS validity
  - $abs\left(\langle HWS \rangle_{vec} - \langle HWS \rangle_{vec,\ sonic}\right) < 0.3\ m.s^{-1}$
  - Unpredictable reference measurement accidents yielding outliers are removed, e.g. a bird sitting on sonic anemometer.
- Flow tilt:
  - $\langle \varphi_{flow} \rangle \in [-2°\ ;\ 2°]$
  - to limit the contribution of the wind vector's vertical component to the RWS, that is neglected in the RWS calibration (see 3.1 in [3]).

- Lidar CNR[5]:
  - $\langle CNR \rangle \geq -18\ dB$.
  - To filter out low backscatter signals, which can be due to unpredictable measurement accidents, e.g. the beam hitting a hard target (mast, bird, etc) or fog.
- Lidar tilt:
  - $\langle \varphi_{ind} \rangle \in default \pm 0.06°$.
  - The default value is the indicated tilt at the time of the beam positioning.
  - This filter ensures that the beam is located on average close to its nominal position.
- LOS availability:
  - $LOS_{avail} > 95\%$.
  - Good data availability is required in order to reduce potential biases due to failed measurements.
- Counts:
  - $LOS_{count} = 120$
  - A count is obtained if an attempt to estimate the LOS velocity is made. As the 5-beam Demonstrator returns to the same LOS every 5 seconds, the expected total is 120 regardless of the LOS availability. This filter only removed partial 10-min periods, i.e. with start/stop events.
- Sonic status address (bit number)
  - $\min(StatA_{sonic}) \geq 01$.
  - $StatA_{sonic} = 00$ indicates error codes. Thus, the 10-min period is filtered out if one 00 value is found.
- Wind direction:
  - $\langle \theta \rangle_{vec} \in LOS_{dir} \pm 40°$
  - Filter with respect to the preferred measuring direction of the lidar, and due to the asymmetry of the sonic anemometer's probes. The ±40° sector replicates operational conditions for which nacelle lidars are designed, i.e. flow towards the lidar, and reasonable yaw misalignment of the turbine (not likely to reach a value as high as 40°).
  - Filter only applied starting from step 3.3.3.2.

[5] The -18 dB threshold is somewhat arbitrary and unit specific. The filter may be adjusted.

3.3.3 LOS direction evaluation

The LOS direction evaluation follows the two-step process described in [3]. The LOS direction results are reported for each LOS (3.4.2).

3.3.3.1 Wind direction response fitting – approximate LOS_{dir}

The response of the normalised lidar RWS to the wind direction is fitted to a sine wave. The RWS ($\langle RWS_{norm} \rangle$) is normalised by the cup anemometer HWS projected only in the vertical plane:

$$\langle RWS_{norm} \rangle = \langle RWS \rangle / \left(\langle HWS \rangle_{vect} \cdot \cos \langle \varphi_{physical} \rangle \right) \quad \text{(eq. 7)}$$

The fitting function is obtained using the method of least squares:

$$f_{fit}(\langle \theta \rangle_{vec}) = a_{LOS} \cdot \cos(\langle \theta \rangle_{vec} - \theta_0) + b_{LOS} \quad \text{(eq. 8)}$$

Consequently, three parameters are obtained from the fitting process, i.e. the gain a_{LOS}, the offset b_{LOS}, and the approximate LOS direction θ_0. The gain and offset are only indications of the data quality and expected to be close to respectively 1 and 0. θ_0 is further used in 3.3.3.2.

3.3.3.2 Residual sum of squares (RSS) – accurate LOS_{dir}

To refine the estimation of the LOS direction, the so-called RSS process is applied. The dataset of 10-min averaged data is restricted to wind directions in the range $\theta_0 \pm 40°$. Linear regressions are then performed between $\langle RWS \rangle$ and the reference wind speed projected using angles θ_{proj} contained in the range $\theta_0 \pm 1°$ with a step of e.g. $0.1°$:

$$\langle HWS \rangle_{vec} \cdot \cos\left(\langle \varphi_{physical} \rangle \right) \cdot \cos(\langle \theta \rangle_{vec} - \theta_{proj}) \quad \text{(eq. 9)}$$

The residual sum of squares (RSS) of each linear regression is reported and plotted vs. θ_{proj} (see Figure 18). A 2nd order polynomial is fitted to the obtained curve. The LOS direction LOS_{dir} is the minimum of the parabola.

3.3.4 Calibration results: linear regressions on raw and binned data

The reported calibration relation results are, for each LOS, linear regressions between the RWS and reference measurand $Ref_{eq\ RWS}$, where:

$$Ref_{eq\ RWS} = \langle HWS \rangle_{vec} \cdot \cos\left(\langle \varphi_{physical} \rangle \right) \cdot \cos(\langle \theta \rangle_{vec} - LOS_{dir}) \quad \text{(eq. 10)}$$

Both forced and unforced linear regressions are performed on the filtered 10-min averaged data (referred to as “raw”) and on the corresponding binned data. The binning process is:

- $0.5\ m.s^{-1}$ bin width.
- RWS range $[2.75\,;16.25]\ m.s^{-1}$. The minimum bin ($[2.75\,;3.25]\ \mathrm{m.s^{-1}}$) corresponds to the $4 \cdot \cos 40° \cdot \cos 1.6° \approx 3.06\ m.s^{-1}$ value that can be obtained by projecting the mimimum HWS. Similarly, the $[15.75\,;16.25]\ m.s^{-1}$ bin corresponds to the maximum value of $16\ m.s^{-1}$.
- a bin is considered valid if it contains at least 3 data points.

Note: the retained calibration relation is the forced regression of the binned data (see 4.5 in [3]).

3.4 Calibration results

3.4.1 Calibration datasets

The distributions of valid 10-minute averaged RWS data – i.e. after filtering – are plotted for each beam (Figure 17). The mean RWS and number of valid data points are given on the top right of the graphs.

The completion criterion for the calibration of one beam is typically that wind speed bins between 4 and 12 m/s are valid (≥ 30min data in bin). However, meeting such a criterion mainly depends on atmospheric conditions and may sometimes be difficult to achieve. Note that this empirical criterion is not met for LOS3 with the maximum valid bin corresponding to $10.5\ m.s^{-1}$.

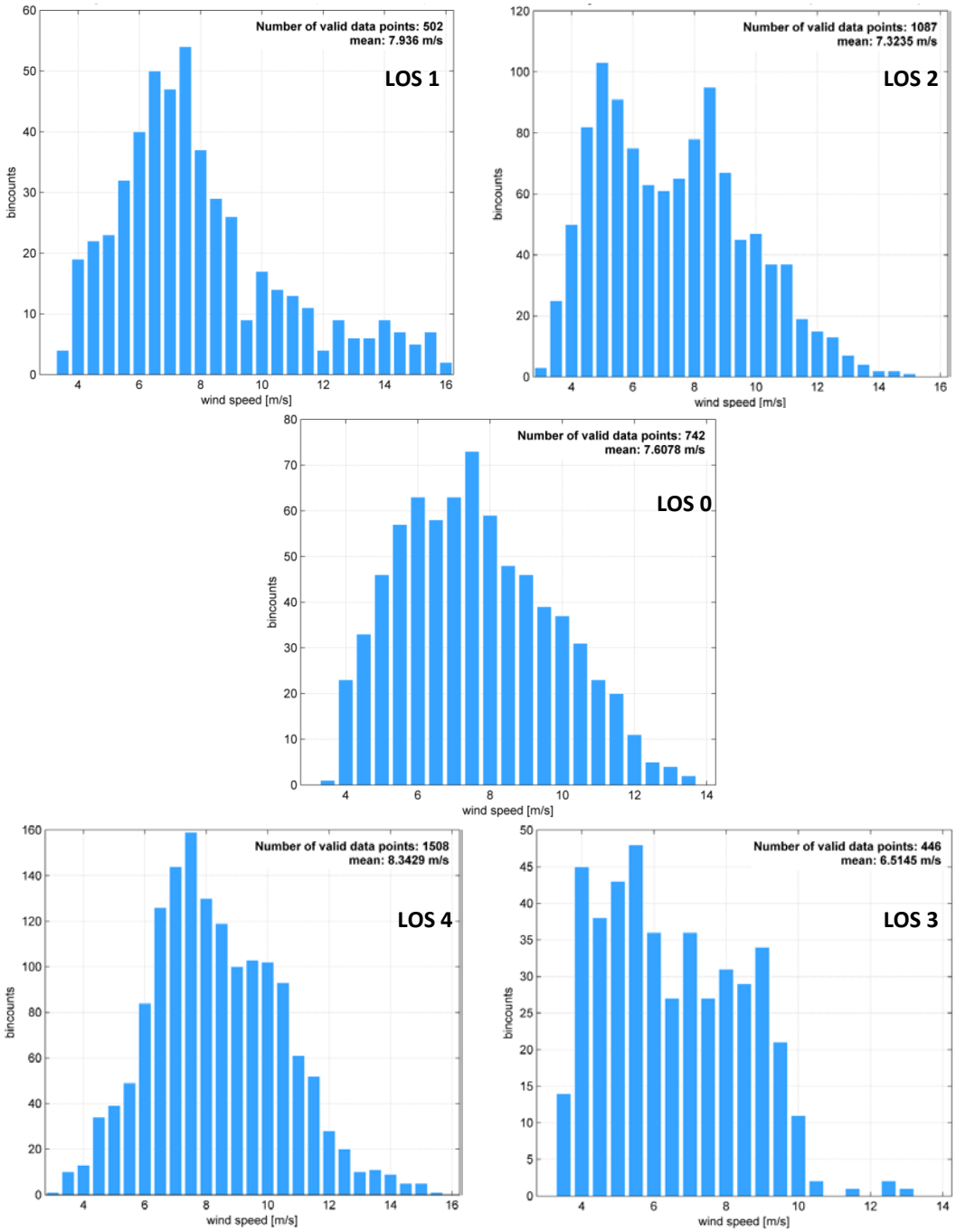

Figure 17. Distributions of radial wind speeds after filtering

3.4.2 LOS directions

Figure 18 shows the results of the two-step LOS direction estimation process, with the fitting coefficients in the top left of the graphs. For all 5 beams, the final LOS direction is 286.01°±0.05°.

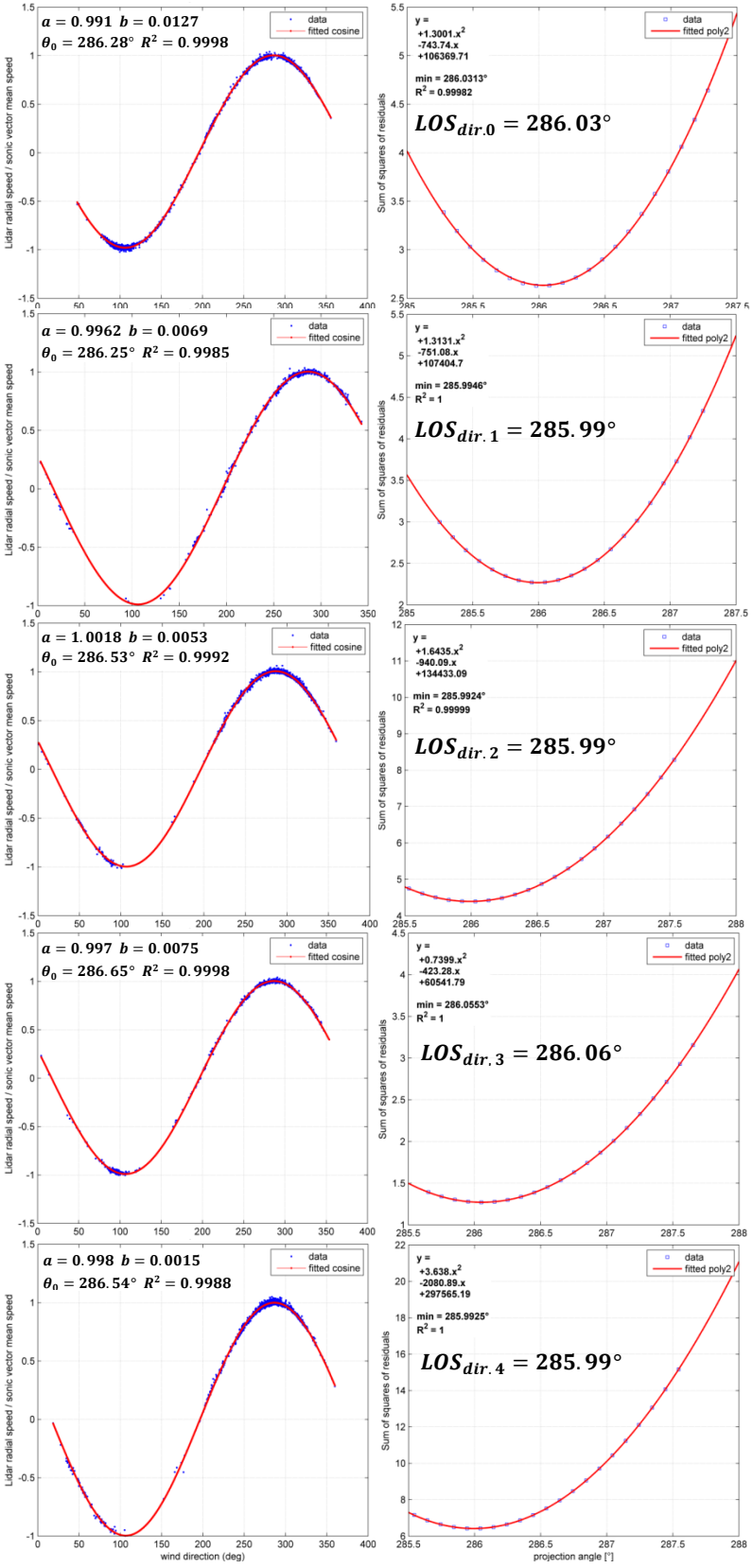

Figure 18. LOS direction evaluation using the cosine fitting (left) and RSS process (right)

3.4.3 Linear regressions

Scatter plots of both raw 10-minute and binned RWS data are shown together with the corresponding forced and unforced linear regression results (Figure 19).

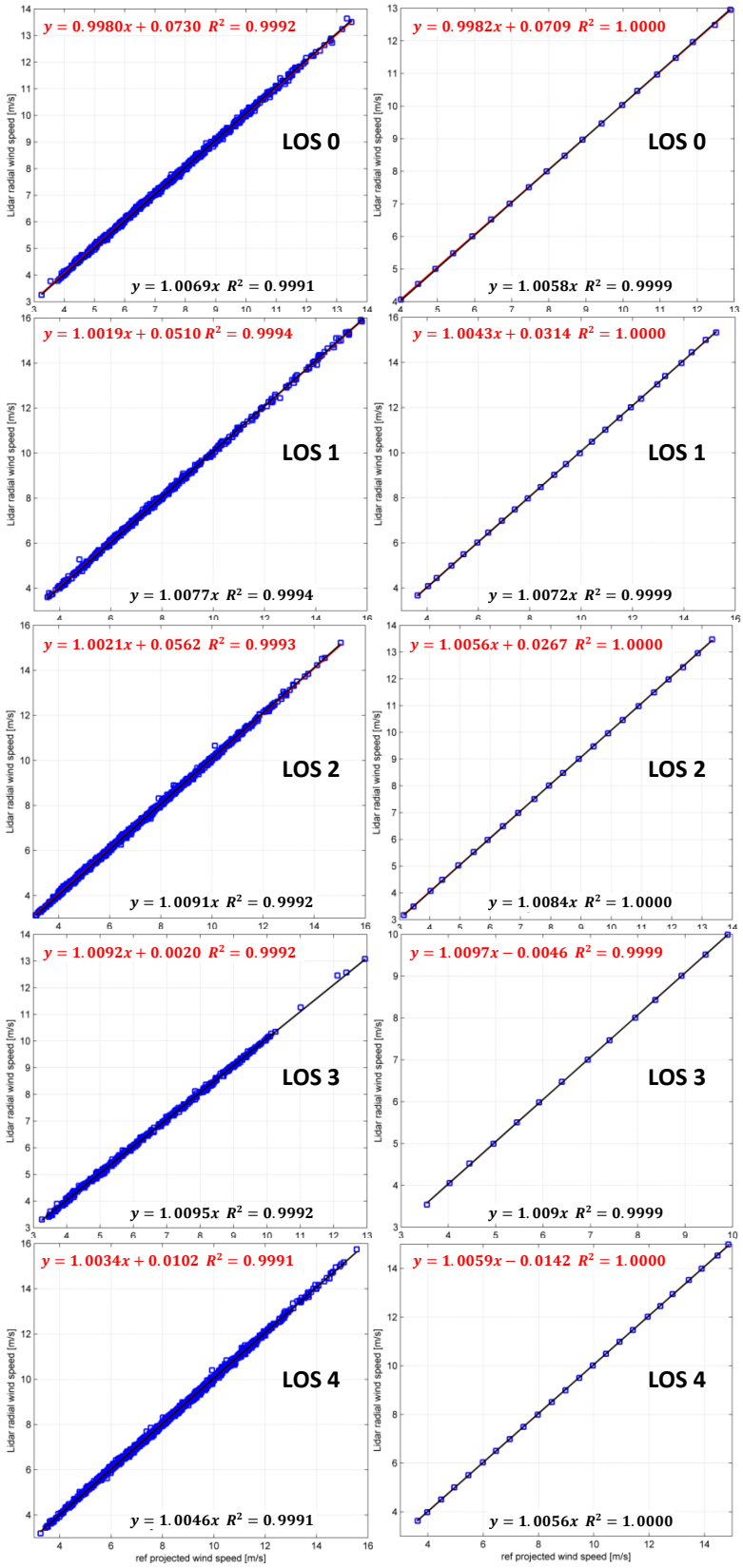

Figure 19. RWS calibration results: 10-minute averaged (left) and binned (right) data

3.4.4 Summary of calibration results

Table 4 summarises the calibration results. **Only the forced regression coefficients on the binned data are given since this corresponds to the selected calibration relation** for the derivation of RWS measurement uncertainties (see 5.7 in [3]).

Table 4. Summary of calibration results – linear regressions (binned RWS vs. reference)

		LOS 0	LOS 1	LOS 2	LOS 3	LOS 4
LOS direction		286.03°	285.99°	285.99°	286.06°	285.99°
Number of valid data points		742	502	1087	446	1508
Forced regression on binned data	Gain	1.0058	1.0072	1.0084	1.0090	1.0056
	R^2	0.9999	0.9999	1.0000	0.9999	1.0000

NB: Annex E provides detailed calibration results tables on both 10-minute and binned data. The results are presented using the cup anemometer for reference wind speed measurements (preferred method). Similar tables obtained by applying the entire calibration using the sonic anemometer only – i.e. both for HWS and wind direction – as reference measurement instrument are provided for information.

3.5 Further investigations

3.5.1 RWS measurement error sensitivity analysis

As explained in [3] (chapter 5.2 "The question of repeatability"), the field calibration of lidars is performed in atmospheric and thus uncontrollable conditions. Based on 10-min averaged data, the influence of external parameters on the RWS measurement error, defined as $\Delta RWS = \langle RWS \rangle - Ref_{eq\ RWS}$, is investigated. The studied parameters are:

- temperature ($T_{abs,2m}$): absolute, measured at 2m a.g.l. on a mast located close to the lidar position ;
- HWS $\langle HWS \rangle_{vect}$;
- turbulence intensity: obtained from the reference cup anemometer, $TI = \sigma_{HWS}/\langle HWS \rangle$;
- wind direction $\langle \theta \rangle_{vec}$;
- flow tilt angle: φ_{flow} measured by the reference sonic anemometer ;
- lidar tilt: indicated value (not corrected)

Annex G displays the results of the sensitivity analysis for all 5 beams in the form of scatter plots of ΔRWS (in $m.s^{-1}$) vs. the aforementioned external parameters. No significant sensitivity neither to temperature[6] (Figure 26), turbulence intensity (Figure 27), HWS (Figure 28) nor the lidar tilting[7] (due to aerodynamic loading of the optical head ; see Figure 31) can be observed. note the low range of temperatures observed in Winter conditions The RWS measurement error seems on the other hand to be sensitive to both the flow tilt angle (Figure 30) and the wind direction (Figure 29). Indeed, scattered parabolic trends centered respectively

[6] Note the low range of temperatures obversed in Figure 26, corresponding to Winter meteorological conditions in Denmark.

[7] The sensitivity to the tilting of the lidar may be further studied if a calibration was to be performed with the lidar placed on a platform at higher height a.g.l. (e.g. 80m). The larger tilting of the met. mast would then add an uncertainty component that is expected to be of the same order of magnitude as measuring from the ground with a highly tilted beam. Alternatively, the uncertainty component on the RWS from the tilting of the mast could be modelled. However, no detailed investigation of the deflections of e.g. free standing masts is available to our knowledge.

on 0° (i.e. horizontal flow) and on ~285° corresponding to the LOS direction can be identified. It is very possible that those sensitivities are due to the cup rather than the 5-beam Demonstrator lidar, as similar sensitivities were observed for other lidar units.

3.5.2 Sensed range and timelag verification

The aim of the sensed range and timelag verification (see §4.4.7 [4]) is to provide evidence that the lidar senses the wind at the correct range and that the lidar measurements are synchronised with the reference instruments (mast data acquisition system).

The analysis is performed using realtime data and thus can be time-consuming. For each valid 10-min period[8], the cross-correlation between the lidar RWS and the projected reference wind speed (downsampled to the lidar measurement frequency) is estimated at each range and for a number of timelags (e.g. ±15 seconds). The result is a matrix of correlation coefficients: with 10 ranges and ±15 seconds (step of 1s), the matrix size is 10×31. The sensed range and timelag are assumed to be obtained for the highest correlation coefficient in the matrix.

The sensed range and timelag process is performed for all five LOS. The main results are presented using LOS0 (see Annex H for other LOS results): the sensed range, sensed timelag and maximum correlation coefficient are presented in scatter plots against HWS and wind direction (see Figure 20).

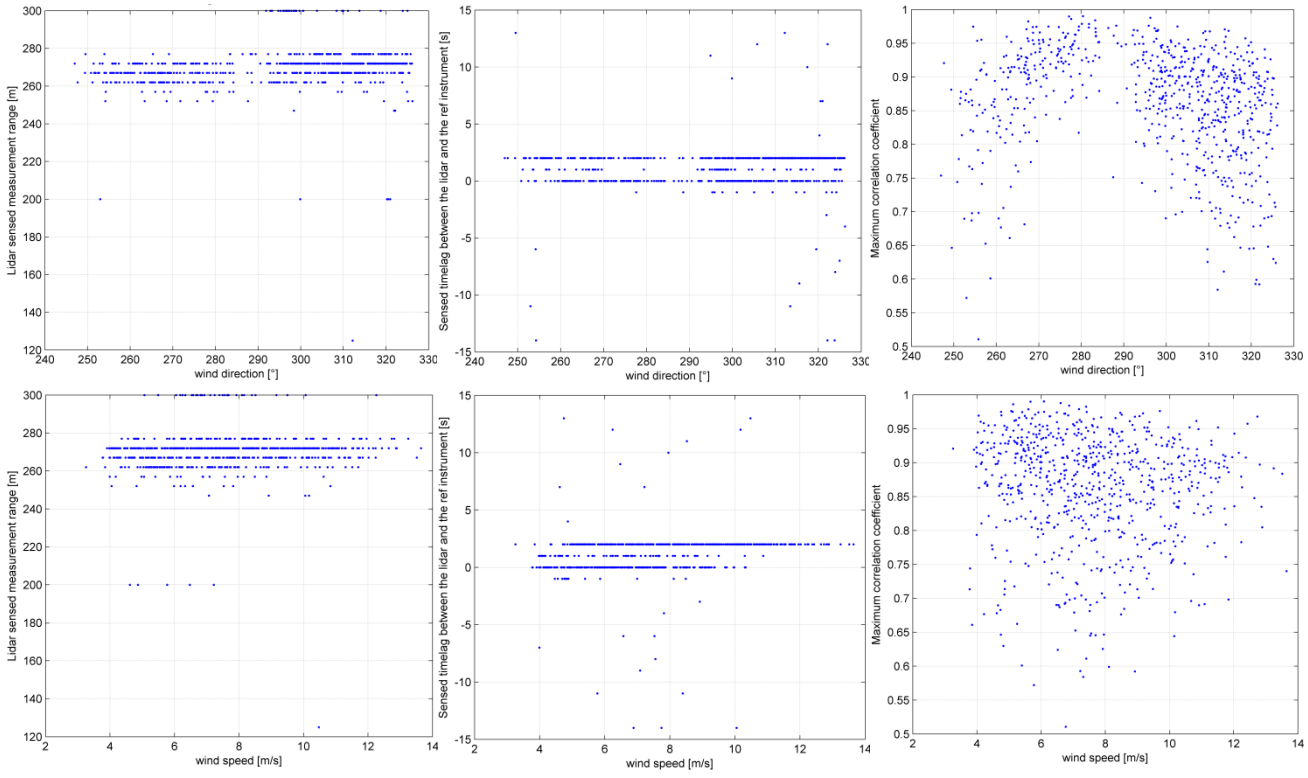

Figure 20. Sensed range and timelag verification for LOS 0. Left: sensed range [m]. Center: timelag [s]. Right: maximum correlation coefficient [-]. Top: vs. wind direction [°]. Bottom: vs. HWS [m.s^{-1}]

[8] Alternatively, a number of randomly picked valid (i.e. filtered) 10-min periods can be used.

The configured and thus expected sensed range for LOS 0 is 262m (252m for the 4 other LOS). The sensed timelag and maximum correlation coefficient should be as close as possible to respectively 0 second and 1.

Figure 20 shows that the sensed range and timelag depend neither on the wind speed nor direction. The sensed range is most of the time 262m, 267m or 272m, and thus reasonably close to the expected value. One can notice a few outliers – e.g. sensed range equals to 200m – probably due to the statiscal nature of this analysis process. The sensed timelag is within [-1 s; +2 s], indicating a good time synchronisation of the lidar with the masts' data acquisition system. Finally, the maximum correlation coefficient shows a large scatter, but for most of the 10-min periods, a correlation coefficient > 0.80 is observed. The highest values of the maximum correlation coefficient seem to be obtained for wind direction close to the LOS direction (~286°, see Figure 20, top right), with a scattered parabolic trend. This trend also appears in the results obtained for the four other beams (Annex H), particularly for LOS 4.

Table 5 below provides a summary of the sensed range and timelag verification results for all 5-beams. The indicated intervals correspond to visual observations, not statistics.

Table 5. Summary of sensed range and timelag verification results

	LOS 0	**LOS 1**	**LOS 2**	**LOS 3**	**LOS 4**
Sensed range [m]	$\sim[262; 272]$	$\sim[252; 272]$	$\sim[257; 267]$	$\sim[257; 267]$	$\sim[252; 262]$
Sensed timelag [s]	$\sim[0; +2]$	$\sim[0; +1]$	$+1$	$+1$	$\sim[0; +2]$
Max. correlation coefficient [-]	$\gtrsim 0.80$	$\gtrsim 0.85$	$\gtrsim 0.85$	$\gtrsim 0.85$	$\gtrsim 0.80$

Overall, the sensed range of the 5-beam Demonstrator is slightly larger than the expected range, by approximately 5-10m, corresponding to a sensing height error of 15-30cm. Note that these results are only valid for the unit tested during the calibration.

NB: for LOS1, 2, 3 and 4, the expected sensed range is 252m.

3.5.3 Impact of individual filters

Various filters are applied on the 10-minute averaged data before analysis, as detailed in 3.3.2. They impact the quality of the calibration data (outliers detection) and the duration of the data collection. For each LOS calibration period, their impact is analysed by looking at the number of points removed (Table 6):

- Individually: only one filter is applied. The proportion of points removed from the unfiltered dataset is derived;
- Sequentially: filters are added one after another. The obtained dataset size is compared to the one at the previous step;
- "Wind direction filter + individually": the wind direction sector of interest is systematically used. Other filters are added individually.

Table 6 shows that the "lidar tilt", "counts" and "sonic status address" filter out less than 1% of the data and thus have a negligible impact on the data collection. Note that for LOS 2, the lidar tilt filter removes ~15% of the data. It is mostly due to the constant loading of the optical head at high wind speed ($> 14\ m.s^{-1}$), in combination with the selected nominal lidar tilt angle when positioning the beam (see 3.2).

On average, valid wind directions were observed 65% of the time. This filter directly influences the duration of the calibration: for instance, the calibration of LOS 4 was completed in two weeks when it usually takes between 1 and 1.5 months.

Additionnally, westerly winds typically come at the Høvsøre site with high wind speeds (see Annex F and [9]). The calibrated HWS (4-16 m/s) filter removes roughly 15% of the data for valid wind directions.

The sonic anemometer measurements prove, as expected, to be affected by winds outside of the valid sector: the flow tilt angle and HWS validity filters remove respectively 35-50% and 4-10% of the data when all wind directions are used vs. 10-20% and 1-8% in the valid sector.

Note: in the case where the wind direction reference instrument is a wind vane instead of a sonic anemometer, the HWS validity and flow tilt angle filters cannot be applied. These filters have a negligible impact on the calibration results. If no HWS validity filter is applied, the calibration relation results, i.e. the gain on the forced binned data, differ by less than 0.03%. If no flow tilt angle is applied, these results vary by ~0.05%.

Finally, the LOS availability 95% threshold filters out ~15% of the data and is insignificantly sensitive to wind direction. A similar proportion of data is filtered out when both filters are applied individually. Nearly no data is removed by the CNR filter when applied sequentially. It can be thus be observed that the LOS availability and CNR filters overlap. Indeed too low CNR means inability for the lidar to estimate the RWS which then results in lower availability.

Table 6. Filters analysis of the RWS calibration datasets

		Individual		WDir + Individual		Sequential	
	Filter name	pts removed		pts removed		pts removed	
LOS 0 - unfiltered dataset: 5984 pts	Wind direction	4711	79%	-	-	4711	79%
	calibrated HWS	1300	22%	163	13%	163	13%
	Flow tilt angle	2698	45%	151	12%	114	10%
	HWS validity (outlier detection)	258	4%	17	1%	9	1%
	LOS availability	1479	25%	305	24%	243	25%
	Lidar CNR	849	14%	112	9%	0	0%
	Lidar tilt	0	0%	0	0%	0	0%
	Counts	11	0%	4	0%	2	0%
	Sonic status address	7	0%	0	0%	0	0%
LOS 1 - unfiltered dataset: 3516 pts	Wind direction	2347	67%	-	-	2347	67%
	calibrated HWS	1448	41%	342	29%	342	29%
	Flow tilt angle	1730	49%	202	17%	161	19%
	HWS validity (outlier detection)	403	11%	97	8%	31	5%
	LOS availability	885	25%	359	31%	133	21%
	Lidar CNR	359	10%	101	9%	0	0%
	Lidar tilt	0	0%	0	0%	0	0%
	Counts	0	0%	0	0%	0	0%
	Sonic status address	21	1%	1	0%	0	0%
LOS 2 - unfiltered dataset: 4419 pts	Wind direction	2465	56%	-	-	2465	56%
	calibrated HWS	957	22%	197	10%	197	10%
	Flow tilt angle	1516	34%	211	11%	170	10%
	HWS validity (outlier detection)	212	5%	67	3%	23	1%
	LOS availability	728	16%	272	14%	204	13%
	Lidar CNR	680	15%	223	11%	31	2%
	Lidar tilt	532	12%	298	15%	241	18%
	Counts	2	0%	1	0%	1	0%
	Sonic status address	4	0%	0	0%	0	0%
LOS 3 - unfiltered dataset: 3421 pts	Wind direction	2685	78%	-	-	2685	78%
	calibrated HWS	721	21%	182	25%	182	25%
	Flow tilt angle	1681	49%	136	18%	88	16%
	HWS validity (outlier detection)	273	8%	25	3%	6	1%
	LOS availability	814	24%	16	2%	11	2%
	Lidar CNR	521	15%	1	0%	0	0%
	Lidar tilt	0	0%	0	0%	0	0%
	Counts	12	0%	4	1%	3	1%
	Sonic status address	2	0%	0	0%	0	0%
LOS 4 - unfiltered dataset: 3599 pts	Wind direction	1446	40%	-	-	1446	40%
	calibrated HWS	600	17%	125	6%	125	6%
	Flow tilt angle	1211	34%	292	14%	274	14%
	HWS validity (outlier detection)	365	10%	183	8%	66	4%
	LOS availability	404	11%	255	12%	179	11%
	Lidar CNR	24	1%	12	1%	1	0%
	Lidar tilt	0	0%	0	0%	0	0%
	Counts	2	0%	1	0%	0	0%
	Sonic status address	2	0%	0	0%	0	0%
ALL LOSs - unfiltered datasets: 20939 pts	Wind direction	13654	65%	-	-	13654	65%
	calibrated HWS	5026	24%	1009	14%	1009	14%
	Flow tilt angle	8836	42%	992	14%	807	13%
	HWS validity (outlier detection)	1511	7%	389	5%	135	2%
	LOS availability	4310	21%	1207	17%	770	14%
	Lidar CNR	2433	12%	449	6%	32	1%
	Lidar tilt	532	3%	298	4%	241	5%
	Counts	27	0%	10	0%	6	0%
	Sonic status address	36	0%	1	0%	0	0%

Chapter 4

4 Measurement uncertainties

The procedure developed to assess the RWS measurement uncertainties of nacelle lidars is detailed in chapter 5 of [3]. It is based on the GUM methodology (see [6]) and thus relies on the law of propagation of uncertainties.

Consequently, this section only provides the list of uncertainty components, their numeric values employed to derive the RWS measurement uncertainty, and finally the uncertainties results for each LOS.

4.1 RWS uncertainty components

4.1.1 Reference instruments uncertainty sources

The reference instruments are the cup and sonic anemometers, providing the HWS and wind direction respectively. The assessment of their measurement uncertainties follows the latest IEC 61400-12-1 methodology [8].

The uncertainty sources, which values are specified for a coverage factor $k = 1$, are:

- **For the HWS**
  - **Wind tunnel calibration uncertainty (type B)**:

$$u_{cal} = u_{cal\,1} + \frac{0.01}{\sqrt{3}} \cdot \langle HWS \rangle$$

    Where $u_{cal\,1}$ is taken from the calibration certificate (Annex C), $u_{cal\,1} \approx 0.025\ m.s^{-1}$.
  - **Operational uncertainty (type B)**:

$$u_{ope} = \frac{1}{\sqrt{3}} \cdot cup\ class\ number \cdot (0.05 + 0.005 \cdot \langle HWS \rangle)$$

    The calibration has been performed using a "Thies First Class Advanced" cup anemometer (without heating regulation), classified as a class A0.9 anemometer by Deutsche WindGuard. The atmospheric conditions of the A class are compatible with the Høvsøre test site. Thus, the class number we used is 0.9[9].

  - **Mounting uncertainty (type B)**: see Annex G of [8]

$$u_{mast} = 0.5\% \cdot \langle HWS \rangle$$

- **For the wind direction (type B)**: taken from the calibration certificate (see Annex D)

$$u_{WD} \approx 0.4°$$

[9] Alternatively, a class S may be used.

4.1.2 Calibration process uncertainty sources

The uncertainty sources relative to the calibration measurement process are:

- **LOS direction uncertainty (type B)**:

$$u_{LOS\,dir} = 0.1°$$

- **Uncertainty of physical inclination angle (type B)**:

$$u_{\varphi} = 0.05°$$

- **Beam positioning uncertainty (type B)** resulting in wind speed deviations. The positioning uncertainty is conservatively estimated to $u_H = 10\,cm$. This translates at the mast height of $H = 8.9m$ and with a shear exponent estimated – using HWS measurements at different heights - to $\alpha_{exp} = 0.2$ into a wind speed uncertainty of:

$$u_{pos} = \alpha_{exp} \cdot \frac{u_H}{H} \cdot HWS \approx 0.23\% \cdot \langle HWS \rangle$$

- **Inclined beam and range uncertainty (type B)**: estimated in [3] using the probe length of the 5-beam Demonstrator, a range uncertainty of 5m, and the setup of the RWS calibration to:

$$u_{inc} = 0.052\% \cdot \langle HWS \rangle$$

4.2 RWS Uncertainty results

The uncertainty results correspond to the calibration uncertainty of 10-min averaged RWS measurements performed by the lidar infield.

NB: that the calibration uncertainty is not the total uncertainty of the RWS measurements, but only part of it. Once measuring as a stand-alone instrument, additional components may be relevant depending on the operational conditions (e.g. measurements in complex terrain).

The uncertainty results are presented in details using LOS 0, while Annex I contains similar uncertainty results for all the five LOS. A summary for all LOS is also given in Table 9.

4.2.1 Uncertainty assessment methodology

The RWS uncertainty assessment is performed using a procedure based on the forced linear regression between the lidar RWS and reference quantity values (see “option 2a” in [3], 5.4.2). With this method, the best estimate of the RWS is defined, using the reciprocal of the obtained calibration relation, as:

$$\langle RWS_{BE} \rangle = \frac{\langle RWS_{indicated} \rangle}{a_{binned}}$$

Where $\langle RWS_{indicated} \rangle$ is the lidar indicated 10-min average RWS and a_{binned} is the gain of the forced linear regression between the binned lidar RWS and $Ref_{eq\,RWS}$ (see 3.3.4). $y_m = a_{binned} \cdot Ref_{eq\,RWS}$ is the estimated measurand. I.e. y_m defines the measurement model allowing to, following the GUM methodology, propagate the reference instruments uncertainties to the lidar RWS.

4.2.2 Expanded uncertainty results (LOS 0)

The expanded uncertainties (coverage factor $k = 2$, i.e. defining a 95% confidence interval) are plotted against the RWS bin averages (Figure 21). The expanded uncertainty varies linearly with the wind speed (or bin number), with a coefficient of determination of $R^2 = 0.9984$.

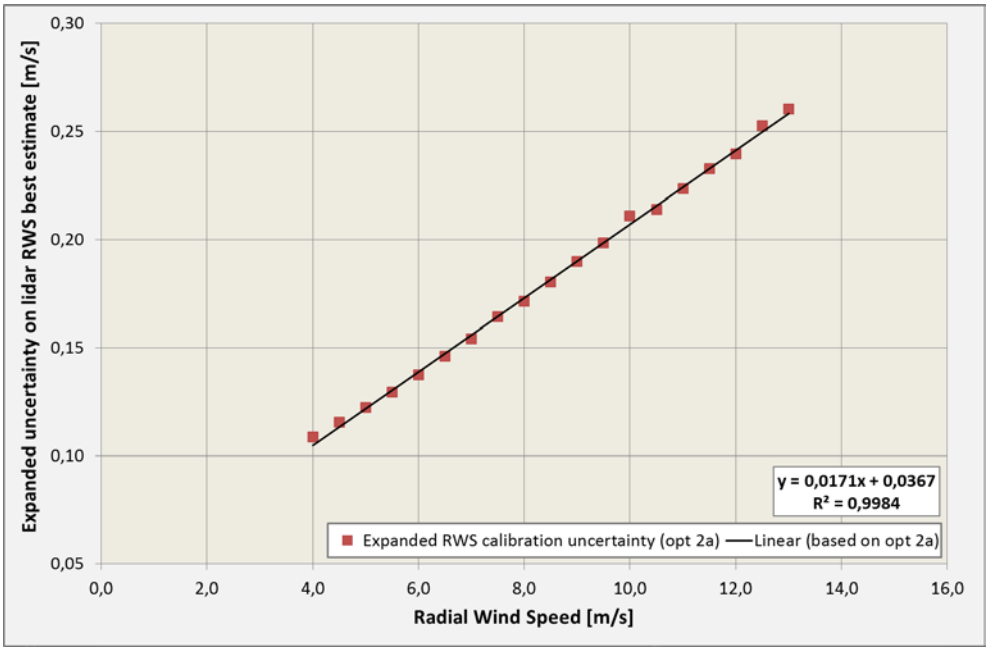

Figure 21. RWS calibration expanded uncertainty (LOS 0)

Figure 22 shows the expanded uncertainty in error bars together with the binned calibration results.

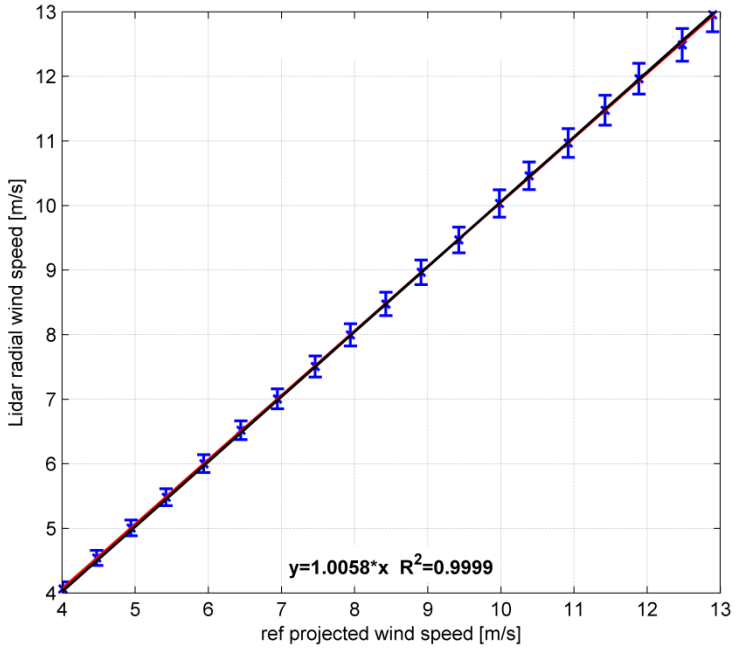

Figure 22. RWS calibration expanded uncertainty results in error bars (LOS 0)

4.2.3 Analysis of uncertainty components (LOS 0)

The two tables below provide the values of the uncertainty components used in the uncertainty assessment:

- Table 7:
  - Columns 4-6: uncertainty components contributing to $Ref_{eq\ RWS}$
  - Column 7: combined uncertainty on $Ref_{eq\ RWS}$ (coverage factor $k = 1$)
  - Columns 8-10: uncertainty components contributing to y_m and combined uncertainty on y_m. Note that U_{c,y_m} is the total RWS calibration uncertainty ($k = 1$).
- Table 8:
  - Columns 4-8: uncertainty components contributing to $\langle HWS \rangle$
  - Column 9: combined uncertainty on $\langle HWS \rangle$ (k=1).

Table 7. Analysis of uncertainty components for y_m and $Ref_{eq\ RWS}$ (LOS 0)

1	2	3	4	5	6	7	8	9	10
Bin	Lower RWS	Upper RWS	U HWS to ref	U tilt to ref	U WDrel to ref	Uc ref	U ym ref	U ym gain	Uc ym
-	[m/s]	[m/s]	[m/s]	[m/s]	[m/s]	[m/s]	[m/s]	[m/s]	[m/s]
…	…	…	…	…	…	…	…	…	…
10	4,75	5,25	0,0588	0,0001	0,0156	0,0608	0,0611	0,0035	0,0612
11	5,25	5,75	0,0624	0,0001	0,0155	0,0643	0,0647	0,0038	0,0648
12	5,75	6,25	0,0664	0,0001	0,0157	0,0682	0,0686	0,0042	0,0687
…	…	…	…	…	…	…	…	…	…
25	12,25	12,75	0,1164	0,0003	0,0465	0,1253	0,1261	0,0088	0,1264
26	12,75	13,25	0,1197	0,0003	0,0484	0,1291	0,1299	0,0091	0,1302
…	…	…	…	…	…	…	…	…	…

Table 8. Analysis of uncertainty components for $\langle HWS \rangle_{vec}$ (LOS 0)

1	2	3	4	5	6	7	8	9
Bin	Lower RWS	Upper RWS	U cal tot	U ope tot	U mast	U pos	U inc	Uc HWS
-	[m/s]	[m/s]	[m/s]	[m/s]	[m/s]	[m/s]	[m/s]	[m/s]
…	…	…	…	…	…	…	…	…
10	4,75	5,25	0,0400	0,0400	0,0270	0,0124	0,0028	0,0639
11	5,25	5,75	0,0420	0,0411	0,0292	0,0134	0,0030	0,0670
12	5,75	6,25	0,0443	0,0424	0,0317	0,0146	0,0033	0,0706
…	…	…	…	…	…	…	…	…
25	12,25	12,75	0,0851	0,0625	0,0703	0,0323	0,0073	0,1311
26	12,75	13,25	0,0878	0,0638	0,0728	0,0335	0,0076	0,1351
…	…	…	…	…	…	…	…	…

Figure 23 illustrates the uncertainty assessment procedure in the form of a "tree" structure. The analysis of the contributions[10] of each component to the next level of uncertainties shows that:

- The reference quantitiy value $Ref_{eq\ RWS}$ uncertainty accounts for 99% of the combined uncertainty on y_m;
- ~90% of $u_{c,Ref_{eq\ RWS}}$ is related to the HWS uncertainty;
- ~95% of the HWS uncertainty is due to the calibration, operational and mast uncertainties, and thus the calibration process uncertainty accounts for the remaining 5% with u_{inc} and u_{pos}.

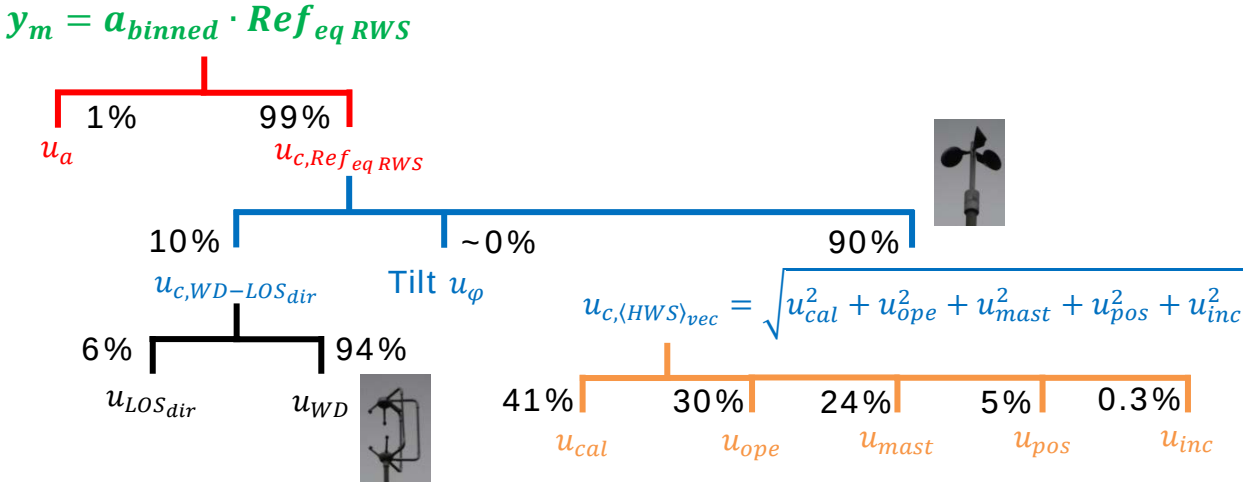

Figure 23. The "tree" structure of the uncertainty assessment methodology

[10] The contributions (in %) provided in Figure 23 correspond to the calibration results of LOS0. Other LOS show similar orders of magnitude.

4.2.4 Summary of calibration uncertainty results (all LOS)

Table 9 provides bin-wise expanded uncertainties for each LOS and with a coverage factor $k = 2$ ($\equiv 95\%$ confidence interval assuming normal distribution of uncertainties). In each bin, the expanded uncertainties are expressed in $m.s^{-1}$ and $\%$ of the bin center.

Table 9. Summary of calibration uncertainty results – bin-wise expanded uncertainties

Bin	RWS bin center [m/s]	LOS 0		LOS 1		LOS 2		LOS 3		LOS 4	
		m/s	*%*	*m/s*	*%*	*m/s*	*%*	*m/s*	*%*	*m/s*	*%*
6	[2.75; 3.25[	0,088	2,93%	0,093	3,09%	0,094	3,13%	0,093	3,11%	0,092	3,07%
7	[3.25; 3.75[	0,096	2,75%	0,102	2,91%	0,099	2,83%	0,101	2,89%	0,101	2,89%
8	[3.75; 4.25[	0,109	2,72%	0,109	2,73%	0,109	2,73%	0,109	2,73%	0,107	2,68%
9	[4.25; 4.75[	0,115	2,56%	0,114	2,53%	0,115	2,56%	0,116	2,58%	0,115	2,56%
10	[4.75; 5.25[	0,122	2,45%	0,123	2,46%	0,123	2,46%	0,123	2,46%	0,122	2,44%
11	[5.25; 5.75[	0,130	2,36%	0,130	2,36%	0,131	2,38%	0,130	2,36%	0,130	2,36%
12	[5.75; 6.25[	0,137	2,29%	0,139	2,32%	0,139	2,32%	0,138	2,30%	0,138	2,30%
13	[6.25; 6.75[	0,146	2,25%	0,145	2,23%	0,147	2,26%	0,145	2,23%	0,145	2,23%
14	[6.75; 7.25[	0,154	2,20%	0,153	2,19%	0,154	2,20%	0,154	2,20%	0,154	2,20%
15	[7.25; 7.75[	0,164	2,19%	0,161	2,15%	0,164	2,19%	0,163	2,17%	0,162	2,16%
16	[7.75; 8.25[	0,171	2,14%	0,172	2,15%	0,170	2,13%	0,170	2,13%	0,171	2,14%
17	[8.25; 8.75[	0,180	2,12%	0,179	2,11%	0,177	2,08%	0,178	2,09%	0,179	2,11%
18	[8.75; 9.25[	0,190	2,11%	0,187	2,08%	0,185	2,06%	0,183	2,03%	0,187	2,08%
19	[9.25; 9.75[	0,199	2,09%	0,193	2,03%	0,193	2,03%	0,191	2,01%	0,195	2,05%
20	[9.75; 10.25[	0,211	2,11%	0,205	2,05%	0,200	2,00%	0,198	1,98%	0,202	2,02%
21	[10.25; 10.75[	0,214	2,04%	0,210	2,00%	0,209	1,99%	0,207	1,97%	0,209	1,99%
22	[10.75; 11.25[	0,223	2,03%	0,219	1,99%	0,218	1,98%	0,215	1,95%	0,216	1,96%
23	[11.25; 11.75[	0,233	2,02%	0,228	1,98%	0,224	1,95%	0,222	1,93%	0,223	1,94%
24	[12.75; 12.25[	0,239	2,00%	0,233	1,94%	0,231	1,93%	0,230	1,91%	0,233	1,94%
25	[12.25; 12.75[	0,253	2,02%	0,241	1,93%	0,240	1,92%	0,237	1,90%	0,238	1,90%
26	[12.75; 13.25[	0,260	2,00%	0,250	1,92%	0,247	1,90%	0,245	1,88%	0,245	1,88%
27	[13.25; 13.75[	0,267	1,98%	0,254	1,88%	0,261	1,93%	0,253	1,87%	0,255	1,89%
28	[13.75; 14.25[	0,276	1,97%	0,263	1,88%	0,264	1,89%	0,260	1,86%	0,263	1,88%
29	[14.25; 14.75[	0,284	1,96%	0,270	1,86%	0,272	1,88%	0,268	1,85%	0,272	1,88%
30	[14.75; 15.25[	0,293	1,95%	0,278	1,85%	0,280	1,87%	0,275	1,84%	0,277	1,85%
31	[15.25; 15.75[	0,301	1,94%	0,285	1,84%	0,288	1,86%	0,283	1,83%	0,286	1,85%
32	[15.75; 16.25[	0,310	1,94%	0,295	1,84%	0,295	1,85%	0,291	1,82%	0,294	1,84%

As the calibration is performed in uncontrolled conditions, the criteria on the minimum number of points per bin may not be met in certain bins. In those bins (shown in red), no uncertainties are obtained experimentally and the uncertainty values may be extrapolated using the linear regressions previously obtained (see e.g. Figure 21 or Table 10).

For example, in the case of LOS 0, the extrapolation formula is:

$$U_{exp,0} = 0.01706 \cdot RWS\ bin\ center + 0.03667 \quad [m.s^{-1}]$$

Table 10. Summary of calibration uncertainty results – linear regressions coefficients (expanded uncertainties vs. RWS bin center)

	LOS 0	LOS 1	LOS 2	LOS 3	LOS 4
Gain	0.01706	0.01556	0.01566	0.01517	0.01552
Intercept	0.03667	0.04590	0.04485	0.04763	0.04568
R^2	0.9984	0.9991	0.9993	0.9991	0.9996

4.3 Deriving uncertainties of reconstructed parameters: example HWS from a "4-beam" nacelle lidar

In this paragraph, the principles of how to combine the uncertainties from different LOS are exemplified through an arbitrary reconstruction algorithm. The reconstructed parameter example is the horizontal wind speed derived from a "4-beam" nacelle lidar, i.e. LOS0 is discarded.

The methodology to obtain the uncertainty of the reconstructed parameter is based on the GUM ([6]). The degree of correlation between the various calibration uncertainty components (see 4.1) is discussed, and the impact on the total uncertainty on the reconstructed parameter investigated.

In terms of uncertainties, when considering correlated or uncorrelated uncertainties, the question to answer is: when the RWS along one beam i is measured with an unknown error $+a$ due to one uncertainty source (e.g. the cup calibration uncertainty), does beam j makes the same error ($R_{ij} = 1$), an error $-a$ ($R_{ij} = -1$), a partially correlated error ($R_{ij} \in]-1;1[$) or a random error ($R_{ij} = 0$). The authors recommend reading §5.2 in [6], which details the theory of correlated uncertainties and provides metrological examples.

4.3.1 Horizontal wind speed reconstruction

An algorithm to reconstruct the horizontal wind vector via its longitudinal and transverse components, denoted U and V respectively, is described. The algorithm discards the central LOS (beam 0). It uses the top (LOS1 and LOS2) and bottom (LOS3 and LOS4) pairs of beams.

Assuming horizontal flow homogeneity, we first express U_{top} and V_{top}:

$$\begin{cases} U_{top} = \dfrac{(V_{r1} + V_{r2})}{2cos\beta_h cos\beta_v} \\ V_{top} = \dfrac{(V_{r1} - V_{r2})}{2sin\beta_h cos\beta_v} \end{cases}$$

Where V_{rX} is the 10-minute averaged of the RWS along LOS X, β_h and β_v are the horizontal and vertical half-opening angles respectively.

Note: in the case of the Avent 5-beam Demonstrator lidar, $\beta_h = \beta_v = \beta \approx 10.73°$ (see 1.2.2).

Similarly for the bottom pair, LOS1 is substituted by LOS4 and LOS2 by LOS3 (see beam numbering in Figure 3). We obtain:

$$\begin{cases} U_{bot} = \dfrac{(V_{r4} + V_{r3})}{2cos\beta_h cos\beta_v} \\ V_{bot} = \dfrac{(V_{r4} - V_{r3})}{2sin\beta_h cos\beta_v} \end{cases}$$

Assuming linear vertical profiles of U and V, the wind vector components at hub height are:

$$\begin{cases} U_{hub} = \dfrac{U_{top} + U_{bot}}{2} = \dfrac{V_{r1} + V_{r2} + V_{r3} + V_{r4}}{4cos\beta_h cos\beta_v} \\ V_{hub} = \dfrac{V_{top} + V_{bot}}{2} = \dfrac{(V_{r1} - V_{r2}) + (V_{r4} - V_{r3})}{4sin\beta_h cos\beta_v} \end{cases}$$

The horizontal speed at hub height is simply:

$$S_{hub} = \sqrt{U_{hub}^2 + V_{hub}^2}$$

4.3.2 Method to combine radial wind speed uncertainties

For the uncertainties, the simplest model is to take the case of $V_{hub} = 0$, i.e. no yaw misalignment. It can be shown that for small and realistic values of yaw error, the uncertainties of the streamwise component U dominate (since this is by far the largest component numerically) but as yaw error increases, the V uncertainties begin to become significant (because of the term $\sin\beta_h \ll 1$ in the denominator).

For zero yaw error, the horizontal speed is simply the U component:

$$S_{hub} = \frac{V_{r1} + V_{r2} + V_{r3} + V_{r4}}{4cos\beta_h cos\beta_v}$$

The uncertainty of the horizontal speed U(S) will depend critically on the correlation between the uncertainties of the 4 radial speeds. Three different cases are thus investigated hereafter:

- No correlation
- Full correlation
- Partial correlation

4.3.2.1 Case 1: no correlation

For completely uncorrelated uncertainties, and neglecting the contribution of the opening angles to the uncertainty, we will simply have:

$$U(S_{hub}) = \frac{1}{4cos\beta_h cos\beta_v}\sqrt{U(V_{r1})^2 + U(V_{r2})^2 + U(V_{r3})^2 + U(V_{r4})^2}$$

If all 4 radial speed uncertainties are equal and given by $U(V_r)$, this simplifies to:

$$U(S_{hub}) = \frac{U(V_r)}{2cos\beta_h cos\beta_v}$$

$\beta_h = \beta_v = 10.73°$, we obtain: $U(S_{hub}) \approx 52\% \cdot U(V_r)$.

4.3.2.2 Case 2: full correlation

At the other extreme, if all the radial speed uncertainties are fully correlated, the RWS uncertainties must be added arithmetically and we obtain:

$$U(S_{hub}) = \frac{U(V_{r1}) + U(V_{r2}) + U(V_{r3}) + U(V_{r4})}{4cos\beta_h cos\beta_v}$$

If all 4 radial speed uncertainties are equal to $U(V_r)$, then:

$$U(S_{hub}) = \frac{U(V_r)}{cos\beta_h cos\beta_v}$$

which is twice as large as for the uncorrelated case. This shows how important it is to consider the correlation between each component of the different beams' RWS uncertainty.

4.3.2.3 Case 3: partial correlation

In the general case, the RWS uncertainties $U(V_{ri})$ are partially correlated. The cross-correlation matrix R (of size 4x4) provides the degree of correlation between pairs of beams:

$$R = \begin{bmatrix} 1 & r_{12} & r_{13} & r_{14} \\ r_{12} & 1 & r_{23} & r_{24} \\ r_{13} & r_{23} & 1 & r_{34} \\ r_{14} & r_{24} & r_{34} & 1 \end{bmatrix}$$

The non-unit cross-correlation coefficients will have different values for different uncertainty components. Simplifying by considering the correlation between RWSs uncertainties instead of the correlation between individual uncertainty components, the uncertainty on the reconstructed horizontal wind speed is:

$$U(S_{hub}) = \frac{1}{4cos\beta_h cos\beta_v} \sqrt{\sum_{i=1}^{4} U^2(V_{ri}) + 2\sum_{i=1}^{4}\sum_{j=i+1}^{4} R_{ij}U(V_{ri})U(V_{rj})}$$

4.3.3 Correlation between RWS uncertainties

In this paragraph, we discuss which case of the three previously mentioned should be used to combine the RWS uncertainties. For the sake of simplicity, we here assume uncertainty components to be either fully correlated or fully uncorrelated. Considering both the calibration process and the definition of the different uncertainty sources (see 4.1), the following table is obtained:

Table 11. Correlation between RWS uncertainty components

	Calibration relation	Horizontal wind speed					Relative wind direction		Tilt
Symbol	u_a	u_{cal}	u_{ope}	u_{mast}	u_{pos}	u_{inc}	u_{WD}	$u_{LOS_{dir}}$	u_{φ}
Correlated between beams	no	yes	yes	yes	no	yes	yes	yes	yes

The only uncertainty components that we can reasonable assume to be uncorrelated are the beam positioning and calibration relation uncertainties (i.e. uncertainty u_a on the gain of the forced regression on binned data), since obtained independently for each LOS. Additionally, these two components have proven to contribute insignificantly to the total RWS uncertainty and are thus negligible (see Figure 23). The other components are obtained from the same sources (same cup anemometer, same tilt inclinometer, etc) and are thus correlated. Following this table, one might thus choose the 2nd case, i.e. full correlation.

Note: this discussion suggests that reducing the RWS measurement uncertainties of lidars could be achieved by using different wind speed reference instruments calibrated in different wind tunnels and by calibrating each beam at a different site. This highlights the weaknesses of the methodology to assess wind speed uncertainty from cup anemometers that is provided by standards.

Second, the distribution of calibration results observed between different LOSs is much smaller than would be the case if the uncertainties between LOSs (both with the same or different lidar units) were uncorrelated. If the RWS uncertainties were truly uncorrelated, one would expect the width of the distribution of the calibration results to be of a similar size as the RWS uncertainties. This is not the case: the gain values of the forced linear regressions are within a 0.5% range. The explanation can be that either the RWS uncertainties are overestimated (probably due to the cup anemometer) or the narrow distribution is a result of seeing the same (unknown) error repeatedly (correlated uncertainty).

Finally, the fully correlated case is the most conservative of the three. For all those reasons, it is suggested to use case 2 (4.3.2.2) to combine uncertainties of reconstructed parameters.

In practice, once operating on the nacelle of a wind turbine, the lidar will not measure the same values of V_r since the bottom LOSs will sense winds at a lower height than the top LOSs. And, for each 10min a non-zero yaw misalignement is expected. Using fully correlated uncertainties, we would obtain:

$$\begin{cases} U(U_{hub}) = \dfrac{U(V_{r1}) + U(V_{r2}) + U(V_{r3}) + U(V_{r4})}{4cos\beta_h cos\beta_v} \\ U(V_{hub}) = \dfrac{U(V_{r1}) - U(V_{r2}) + U(V_{r3}) - U(V_{r4})}{4cos\beta_h cos\beta_v} \end{cases}$$

As the transverse component V_{hub} should be lower than U_{hub}, a lower uncertainty is also obtained due to the minus signs.

Conclusion

In this document, the calibration of 5-beam Avent Demonstrator lidar is reported in details, both from the methods and results point of views. The 'white box' calibration methodology was employed. For all five beams, calibration results proved to be consistent, with a high level of agreement between the measured radial wind speed and reference quantity values. Sensitivity of the lidar's measurements to environmental parameters was investigated and showed that most environmental parameters do not have a significant impact on the lidar's measurement accuracy. Radial wind speed measurement uncertainties were assessed and the methods to do so explained. An arbitrary example of reconstruction algorithm was finally used to exemplify how to combine the radial wind speed uncertainties and estimate uncertainties on wind parameters.

Traceable measurements to national standards can thus be obtained from the 5-beam Avent Demonstrator lidar using the information contained in this report.

Annexes

Annex A. 3-axis rotating platform

To accurately point the beams of the 5-beam Demonstrator lidar towards a target, a 3-axis rotating platform has been designed by DTU Wind Energy technicians (A. Ramsing Vestergaard). The platform allows both gross and fine adjustments of the tilt and roll of the lidar (Figure 24). The yaw of the platform can also be adjusted.

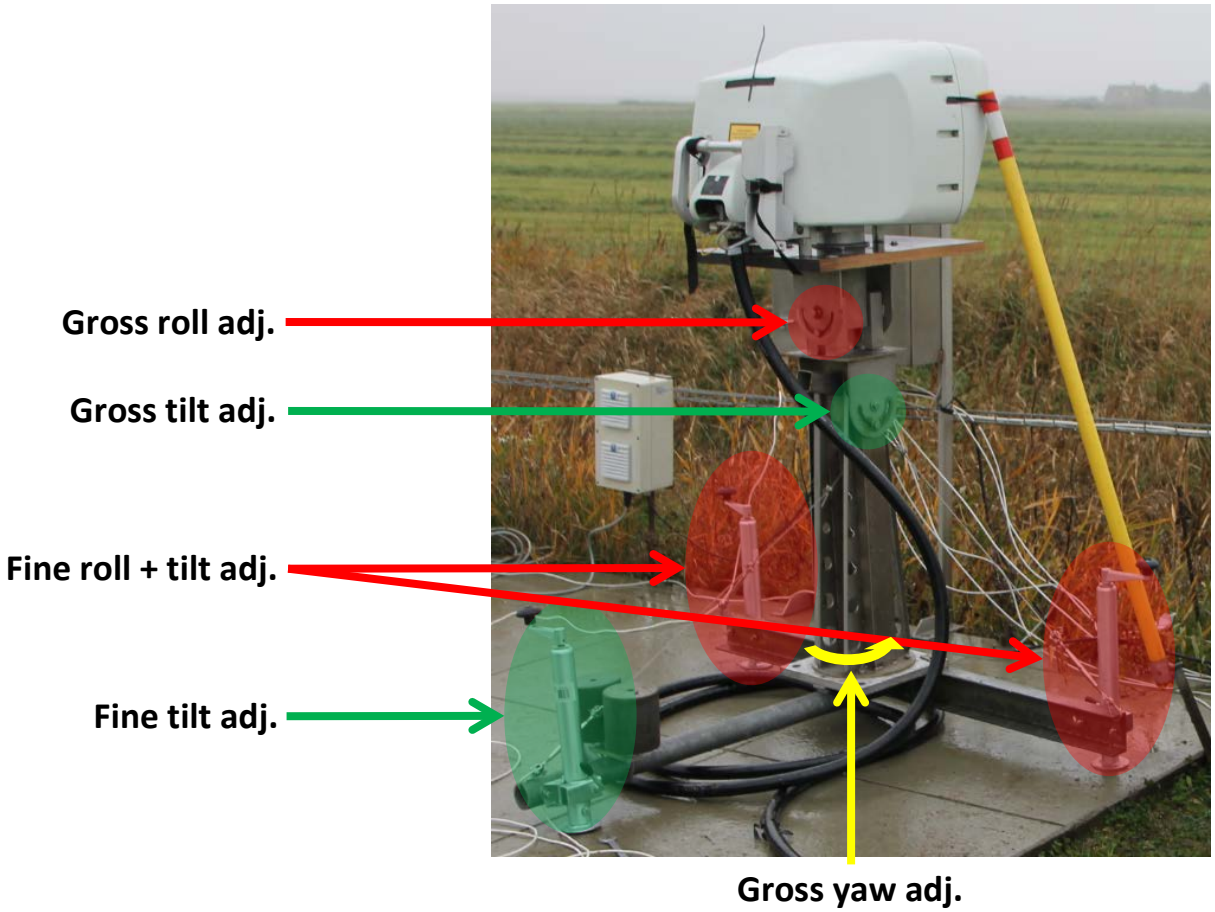

Figure 24. 3-axis rotating platform for accurate beam positioning

Annex B. Calibration of the tilt and roll angles: measurement uncertainties

1. Tilt uncertainties

Using the notation in 2.3.3, the measurement model of the tilt is:

$$\varphi_{mod} = \frac{\varphi_{ref} - offset}{gain}$$

Where:

$$\begin{cases} gain = 1.0123\ [°/°] \\ offset = 0.0471° = 8.2 \cdot 10^{-4} rad \end{cases}$$

This measurement model corresponds to the following correction of the lidar indicated tilt (φ_{BE} is the best estimate of the tilt angle using the lidar indication):

$$\varphi_{BE} = gain \cdot \varphi_{indicated} + offset$$

Applying the GUM methodology to the measurement model, the combined uncertainty $u_{c,\varphi_{mod}}$ is obtained (coverage factor $k = 1$):

$$u_{c,\varphi_{mod}} = \sqrt{\frac{\left(u_{\varphi_{ref}}^2 + u_{offset}^2\right)}{gain^2} + \left(\varphi_{ref} - offset\right)^2 \cdot u_{gain}^2} \qquad \text{(eq. 11)}$$

The uncertainties on the gain and offset are taken as the half-with of the 68% (equivalent to $k = 1$) confidence interval obtained using the unforced linear regression's statistics:

$$\begin{cases} u_{gain} = 0.004874\ [°/°] \\ u_{offset} = 0.003497° = 6.1 \cdot 10^{-5} rad \end{cases}$$

The uncertainty on the reference measurement angle is obtained by applying the GUM methodology to the measurements conducted in 2.3.2. After simplifications, the combined uncertainty is:

$$u_{c,\varphi_{ref}} = \text{atan}\left(\frac{u_{H_0}}{D_{ref-0}}\right) \approx \frac{u_{H_0}}{D_{ref-0}}$$

Conservative estimates of the uncertainties of the beam detection and total station measurements (N, E, Z coordinates) are: $10\ mm$ (beam position). Thus $u_{H_0} = 10mm \cdot \sqrt{2}$. At the distance $D_{ref-0} \approx 30m$, the combined uncertainty on φ_{ref} is $u_{c,\varphi_{ref}} = 0.026°$.

Since $gain \approx 1$, $u_{offset}^2 \ll u_{\varphi_{ref}}^2$ and $\left(\varphi_{ref} - offset\right)^2 \cdot u_{gain}^2 \ll u_{\varphi_{ref}}^2$, (eq. 11) is approximated and simplified to:

$$u_{c,\varphi_{mod}} = u_{\varphi_{ref}}$$

Finally, the expanded uncertainty with a coverage factor $k = 2$ is: $\boldsymbol{U_{\varphi_{BE}} = k \cdot u_{c,\varphi_{mod}} = 0.05°}$.

2. Roll uncertainties

The roll uncertainties are derived using a similar process as for the tilt. The statistics of the unforced linear regression give:

$$\begin{cases} u_{gain} = 0{,}003651\ [°/°] \\ u_{offset} = 0{,}008644° = 1.5 \cdot 10^{-4} rad \end{cases}$$

These two components are also negligible compared to the reference roll ψ_{ref} uncertainty. The uncertainty on the reference measurement angle is obtained by applying the GUM methodology to the measurements conducted in 2.4.2. After simplifications, the combined uncertainty on ψ_{ref} is $u_{\psi_{ref}} = 0.09°$

Finally, the expanded uncertainty is $\boldsymbol{U_{\psi_{BE}} = k \cdot u_{c,\psi_{BE}} = 0.18°}$ with a coverage factor $k = 2$.

Annex C. Calibration certificate of cup anemometer

Deutsche WindGuard
Wind Tunnel Services GmbH, Varel

Deutsche WindGuard

1108/2722

akkreditiert durch die / *accredited by the*

Deutsche Akkreditierungsstelle GmbH

DAkkS Deutsche Akkreditierungsstelle D-K-15140-01-00

als Kalibrierlaboratorium im / *as calibration laboratory in the*

Deutschen Kalibrierdienst DKD

	1323249
	D-K-15140-01-00
Calibration mark	10/2013

Kalibrierschein
Calibration certificate

Gegenstand *Object*	Cup Anemometer
Hersteller *Manufacturer*	Thies Clima D-37083 Göttingen
Typ *Type*	4.3351.10.000
Fabrikat/Serien-Nr. *Serial number*	11116763 2722
Auftraggeber *Customer*	Risoe DTU DK-4000 Roskilde
Auftragsnummer *Order No.*	VT131006
Anzahl der Seiten des Kalibrierscheines *Number of pages of the certificate*	3
Datum der Kalibrierung *Date of calibration*	24.10.2013

Dieser Kalibrierschein dokumentiert die Rückführung auf nationale Normale zur Darstellung der Einheiten in Übereinstimmung mit dem Internationalen Einheitensystem (SI).
Die DAkkS ist Unterzeichner der multilateralen Übereinkommen der European co-operation for Accreditation (EA) und der International Laboratory Accreditation Cooperation (ILAC) zur gegenseitigen Anerkennung der Kalibrierscheine.
Für die Einhaltung einer angemessenen Frist zur Wiederholung der Kalibrierung ist der Benutzer verantwortlich.

This calibration certificate documents the traceability to national standards, which realize the units of measurement according to the International System of Units (SI).
The DAkkS is signatory to the multilateral agreements of the European co-operation for Accreditation (EA) and of the International Laboratory Accreditation Cooperation (ILAC) for the mutual recognition of calibration certificates.
The user is obliged to have the object recalibrated at appropriate intervals.

Datum *Date*	Leiter des Kalibrierlaboratoriums *Head of the calibration laboratory*	Bearbeiter *Person in charge*
24.10.2013	Dipl. Phys. D. Westermann	Technikerin Bilke Engelbrecht

Seite 2
Page

1323249
D-K-15140-01-00
10/2013

Kalibriergegenstand
Object Cup Anemometer

Kalibrierverfahren
Calibration procedure IEC 61400-12-1 – Power performance measurements of electricity producing wind turbines – 2005-12
ISO 3966 – Measurement of fluid in closed conduits – 2008-07

Ort der Kalibrierung
Place of calibration Windtunnel of Deutsche WindGuard, Varel

Messbedingungen
Test Conditions

wind tunnel area [1]	10000 cm²	
anemometer frontal area [2]	230 cm²	
diameter of mounting pipe [3]	34 mm	
blockage ratio [4]	0.023 [-]	
blockage correction [5]	1.000 [-]	

Umgebungsbedingungen
Test conditions

air temperature	22.9 °C	± 0.1 K
air pressure	1017.5 hPa	± 0.3 hPa
relative air humidity	53.7 %	± 2.0 %

Akkreditierung
Accreditation 01/2013

Anmerkungen
Remarks Calibration after refurbishment

Auswertesoftware
Software version 7.58

[1] Querschnittsfläche der Auslassdüse des Windkanals
[2] Vereinfachte Querschnittsfläche (Schattenwurf) des Prüflings inkl. Montagerohr
[3] Durchmesser des Montagerohrs
[4] Verhältnis von 2) zu 1)
[5] Korrekturfaktor durch die Verdrängung der Strömung durch den Prüfling
Anmerkung: Aufgrund der speziellen Konstruktion der Messstrecke ist keine Korrektur nötig.
Remark: Due to the special construction of the test section no blockage correction is necessary

Dieser Kalibrierschein wurde elektronisch erzeugt
This calibration certificate has been generated electronically

Deutsche WindGuard
Wind Tunnel Services GmbH, Varel

Deutsche WindGuard

Seite 3
Page

1323249
D-K-15140-01-00
10/2013

Kalibrierergebnis:
Result:

File:	1323249	
Test Item (1/s)	Tunnel Speed (m/s)	Uncertainty (k=2) (m/s)
82.449	4.018	0.050
124.924	5.986	0.050
169.001	8.019	0.050
212.344	9.996	0.051
256.175	12.024	0.051
298.122	13.974	0.051
342.208	15.956	0.051
321.984	15.015	0.051
277.958	13.013	0.051
233.498	10.981	0.051
190.816	9.023	0.051
147.893	7.033	0.050
103.351	4.980	0.050

Angegeben ist die erweiterte Messunsicherheit, die sich aus der Standardmessunsicherheit durch Multiplikation mit dem Erweiterungsfaktor k=2 ergibt. Sie wurde gemäß DAkkS-DKD-3 ermittelt. Der Wert der Messgröße liegt mit einer Wahrscheinlichkeit von 95 % im zugeordneten Wertintervall.

Die Deutsche Akkreditierungsstelle GmbH ist Unterzeichnerin der multilateralen Übereinkommen der European co-operation for Accreditation (EA) und der International Laboratory Accreditation Cooperation (ILAC) zur gegenseitigen Anerkennung der Kalibrierscheine. Die weiteren Unterzeichner innerhalb und außerhalb Europas sind den Internetseiten von EA (www.european-accreditation.org) und ILAC (www.ilac.org) zu entnehmen.

The expanded uncertainty assigned to the measurement results is obtained by multiplying the standard uncertainty by the coverage factor k = 2. It has been determined in accordance with DAkkS-DKD-3. The value of the measurand lies within the assigned range of values with a probability of 95%.

The DAkkS is signatory to the multilateral agree-ments of the European co-operation for Accredita-tion (EA) and of the International Laboratory Accreditation Cooperation (ILAC) for the mutual recognition of calibration certificates.

Deutsche WindGuard
Wind Tunnel Services GmbH, Varel

Deutsche WindGuard

Anhang
Annex

1323249

1 Detailed Calibration Results

DKD calibration no.	1323249
Body no.	11116763
Cup no.	2722
Date	24.10.2013
Air temperature	22.9 °C
Air pressure	1017.5 hPa
Humidity	53.7 %

Linear regression analysis

Slope	0.04597 (m/s)/(1/s) ±0.00005 (m/s)/(1/s)
Offset	0.2388 m/s ±0.012 m/s
St.err(Y)	0.013 m/s
Correlation coefficient	0.999993

Remarks no

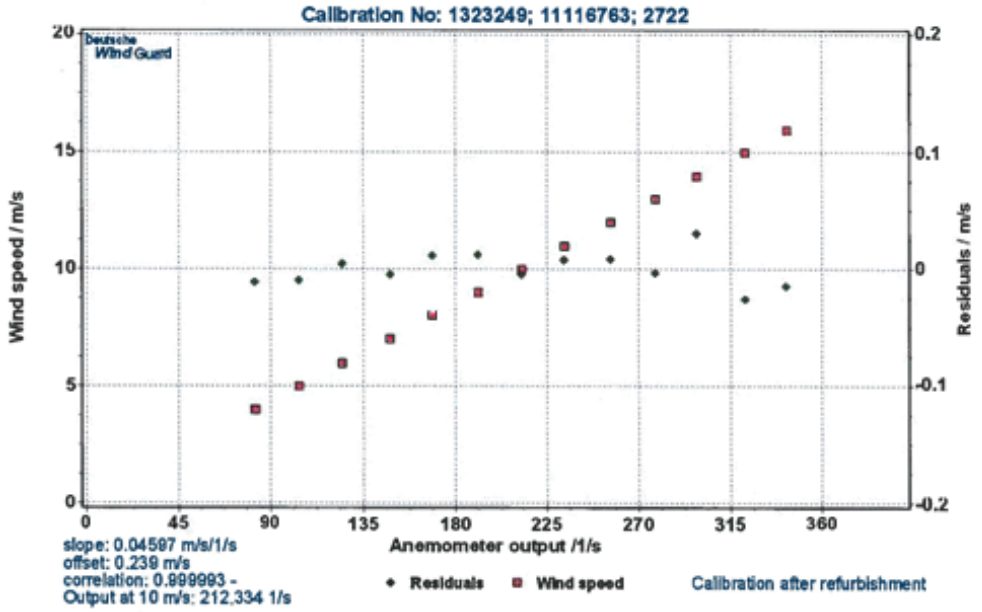

Deutsche WindGuard Wind Tunnel Services is accredited by MEASNET and by the Deutsche Akkreditierungsdienst – DAkkS (German Accreditation Service). Registration: D-K-15140-01-00

Deutsche WindGuard
Wind Tunnel Services GmbH, Varel

Anhang
Annex

1323249

2 Instrumentation

Pos.	Sensor	Manufa.	Type	Range
1	Pitot static tube	Airflow	NPL 8 mm	-
2	Pitot static tube	Airflow	NPL 8 mm	-
3	Pitot static tube	Airflow	NPL 8 mm	-
4	Pitot static tube	Airflow	NPL 8 mm	-
5	Pressure transducer	Setra	C 239	250 Pa
6	Pressure transducer	Setra	C 239	250 Pa
7	Pressure transducer	Setra	C 239	250 Pa
8	Pressure transducer	Setra	C 239	250 Pa
9	El. Barometer	Vaisala	3.11.57.10.000	800hPa -1200 hPa
10	El. Thermometer	Galltec	KPK 1/6-ME	10° C - 40° C
11	El. Humidity sensor	Galltec	KPK 1/6-ME	0-100 %
12	Wind tunnel control	-	-	-
13	CAN-BUS / PC	esd	24 x 16 bit	

Table 1 Description of the data acquisition system
Remark: Last Re-accreditation see page 2

3 Photo of the calibration set-up

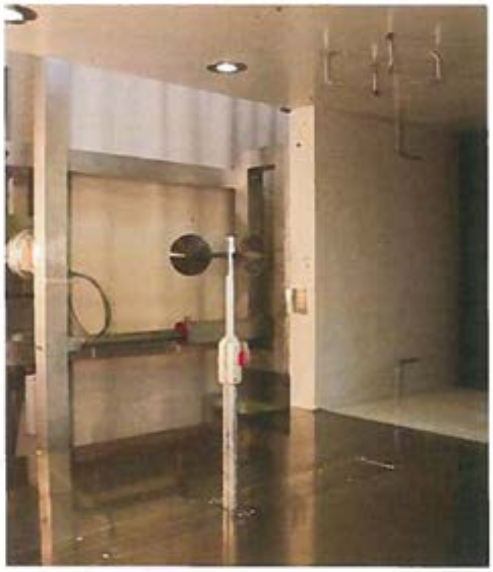

Calibration set-up of the anemometer calibration in the wind tunnel of Deutsche WindGuard, Varel. The anemometer and orientation shown may differ from the calibrated one. Remark: The proportion of the set-up is not true to scale due to imaging geometry.

4 Deviation to IEC procedure

The calibration procedure is in all aspects in accordance with the IEC 61400-12-1 Procedure

5 References

[1] D. Westermann, 2009 – Verfahrensanweisung DKD-Kalibrierung von Windgeschwindigkeitssensoren
[2] IEC 61400-12-1 12/2005 – Power performance measurements of electricity producing wind turbines
[3] ISO 3966 2008 – Measurement of fluid flow in closed conduits

Annex D. Calibration certificate of sonic anemometer, for wind direction, at 0° inflow

Deutsche WindGuard
Wind Tunnel Services GmbH, Varel

Deutsche WindGuard

7820/0845

akkreditiert durch die / *accredited by the*

Deutsche Akkreditierungsstelle GmbH

DAkkS Deutsche Akkreditierungsstelle D-K-15140-01-00

als Kalibrierlaboratorium im / *as calibration laboratory in the*

Deutschen Kalibrierdienst DKD

1322749	
D-K-15140-01-00	
Calibration mark	09/2013

Kalibrierschein
Calibration certificate

Gegenstand *Object*	Sonic Anemometer	
Hersteller *Manufacturer*	Gill Instruments UK-Hampshire S041 9EG	
Typ *Type*	1210R3	
Fabrikat/Serien-Nr. *Serial number*	000078	
Auftraggeber *Customer*	Risoe DTU DK-4000 Roskilde	
Auftragsnummer *Order No.*		VT130930
Anzahl der Seiten des Kalibrierscheines *Number of pages of the certificate*		5
Datum der Kalibrierung *Date of calibration*		13.09.2012

Dieser Kalibrierschein dokumentiert die Rückführung auf nationale Normale zur Darstellung der Einheiten in Übereinstimmung mit dem Internationalen Einheitensystem (SI).
Die DAkkS ist Unterzeichner der multilateralen Übereinkommen der European co-operation for Accreditation (EA) und der International Laboratory Accreditation Cooperation (ILAC) zur gegenseitigen Anerkennung der Kalibrierscheine.
Für die Einhaltung einer angemessenen Frist zur Wiederholung der Kalibrierung ist der Benutzer verantwortlich.
This calibration certificate documents the traceability to national standards, which realize the units of measurement according to the International System of Units (SI).
The DAkkS is signatory to the multilateral agreements of the European co-operation for Accreditation (EA) and of the International Laboratory Accreditation Cooperation (ILAC) for the mutual recognition of calibration certificates.
The user is obliged to have the object recalibrated at appropriate intervals.

Datum *Date*	Leiter des Kalibrierlaboratoriums *Head of the calibration laboratory*	Bearbeiter *Person in charge*
16.09.2012	Dipl. Phys. D. Westermann	Dipl.-Ing. (FH) Catharina Herold

Seite 2 *Page*	1322749 D-K-15140-01-00 09/2013

Kalibriergegenstand
Object
Sonic Anemometer

Ort der Kalibrierung
Place of calibration
Windtunnel of Deutsche WindGuard, Varel

Kalibrierverfahren
Calibration procedure
ASTM 5366-96 Standard Test Method of Measuring the Dynamic Performance of Wind Vanes - 2002
Deutsche WindGuard Verfahrensanweisung Kalibrierung von Windrichtungssensoren

Die messtechnische Bestimmung der angezeigten Windrichtung eines Windrichtungssensors zur Strömungsrichtung im Windkanal erfolgt mit Hilfe einer Dreheinrichtung unterhalb der Messstrecke des Windkanals. Während der Messung wird der Windrichtungssensor kontinuierlich von 0 Grad bis 40 Grad und zurück nach 320 Grad bei konstanter Strömungsgeschwindigkeit gedreht. Die Mittelwertbildung erfolgt in Klassen (Klassenbreite siehe Seite 3).

The measurement of the indicated direction of a wind vane to statically yawed air flow is done with the help of an automatic yaw device installed below the wind tunnel test section. During the measurements, the wind vane is yawed continuously from 0 to 40 degrees and back to 320 degree at constant flow speed. The data are bin-averaged in classes (see page 3).

Umgebungsbedingungen:
Test conditions

air temperature:	24.5 °C
air pressure:	1017.4 hPa
relative air humidity:	56.4 %

Kommentar:
Comment
Tilt orientation: 0 deg

Akkreditierung:
Accreditation
01/2013

Dieser Kalibrierschein wurde elektronisch erzeugt
This calibration certificate has been generated electronically

Deutsche WindGuard
Wind Tunnel Services GmbH, Varel

Deutsche WindGuard

Seite 3
Page

1322749
D-K-15140-01-00
09/2013

Kalibrierergebnis:
Result:

File:	1322749					
Bin	Flow Dir	dir	v_hor	v_ver	Unc	Flow speed
-	deg	deg	m/s	m/s	deg	m/s
1	0.99	0.854	7.940	-0.103	0.8	8.139
2	1.98	1.939	7.950	-0.097	0.8	8.138
3	3.06	2.909	7.944	-0.102	0.8	8.139
4	4.05	4.023	7.952	-0.101	0.8	8.137
5	5.02	5.265	7.950	-0.101	0.8	8.136
6	6.03	6.814	7.963	-0.092	0.8	8.139
7	7.00	7.000	7.956	-0.083	0.8	8.129
8	8.00	7.918	7.964	-0.089	0.8	8.141
9	9.02	8.979	7.969	-0.089	0.8	8.137
10	9.96	9.977	7.965	-0.088	0.8	8.139
11	10.98	11.023	7.954	-0.093	0.8	8.141
12	11.97	12.333	7.948	-0.094	0.8	8.143
13	12.98	13.771	7.960	-0.100	0.8	8.135
14	14.03	14.000	7.965	-0.103	0.8	8.139
15	15.01	15.163	7.959	-0.106	0.8	8.133
16	16.02	16.085	7.964	-0.108	0.8	8.136
17	17.05	17.292	7.969	-0.113	0.8	8.144
18	18.01	18.023	7.968	-0.113	0.8	8.140
19	18.98	19.313	7.972	-0.115	0.8	8.140
20	20.01	20.625	7.965	-0.114	0.8	8.138
21	20.99	21.026	7.971	-0.117	0.8	8.144
22	21.98	22.481	7.977	-0.117	0.8	8.140
23	23.06	23.041	7.982	-0.121	0.8	8.139
24	24.02	24.717	7.972	-0.124	0.8	8.142
25	25.00	25.851	7.984	-0.122	0.8	8.138
26	26.12	26.045	7.969	-0.126	0.8	8.140
27	27.01	27.098	7.965	-0.125	0.8	8.137
28	27.95	27.980	7.966	-0.130	0.8	8.141
29	29.00	29.540	7.967	-0.124	0.8	8.137
30	29.88	29.951	7.961	-0.125	0.8	8.139
31	30.94	31.306	7.979	-0.123	0.8	8.144
32	32.03	32.490	7.978	-0.123	0.8	8.141
33	33.04	33.279	7.970	-0.117	0.8	8.136
34	34.04	34.447	7.989	-0.110	0.8	8.137
35	35.03	35.410	7.994	-0.115	0.8	8.141
36	36.01	37.000	8.000	-0.112	0.8	8.141
37	37.01	37.279	7.998	-0.111	0.8	8.142
38	37.98	39.071	7.990	-0.105	0.8	8.142
39	38.94	39.795	8.005	-0.102	0.8	8.139
40	39.95	40.463	8.002	-0.096	0.8	8.140

Deutsche WindGuard
Wind Tunnel Services GmbH, Varel

Deutsche WindGuard

Seite 4
Page

1322749
D-K-15140-01-00
09/2013

File:	1322749					
Bin	Flow Dir	dir	v_hor	v_ver	Unc	Flow speed
-	deg	deg	m/s	m/s	deg	m/s
41	319.96	319.136	7.996	0.010	0.8	8.140
42	320.93	321.118	8.009	0.006	0.8	8.141
43	321.96	321.933	8.006	0.008	0.8	8.141
44	322.96	322.000	7.993	-0.001	0.8	8.141
45	324.00	322.754	7.985	-0.002	0.8	8.142
46	325.07	324.135	7.996	-0.003	0.8	8.132
47	326.07	325.531	7.998	-0.005	0.8	8.133
48	327.00	326.698	8.004	-0.010	0.8	8.138
49	328.04	328.509	8.002	-0.019	0.8	8.141
50	329.01	328.755	7.991	-0.021	0.8	8.136
51	329.98	329.460	7.992	-0.026	0.8	8.136
52	330.98	330.811	8.001	-0.025	0.8	8.139
53	331.99	331.818	7.967	-0.031	0.8	8.133
54	332.98	332.966	7.966	-0.031	0.8	8.137
55	334.08	333.778	7.985	-0.031	0.8	8.134
56	335.07	335.043	7.987	-0.026	0.8	8.140
57	336.01	335.940	7.984	-0.028	0.8	8.137
58	337.09	336.556	7.986	-0.032	0.8	8.141
59	337.98	337.778	7.985	-0.034	0.8	8.138
60	338.95	338.824	7.985	-0.039	0.8	8.144
61	339.99	340.400	7.981	-0.041	0.8	8.142
62	340.96	340.896	7.970	-0.045	0.8	8.138
63	342.02	341.021	7.966	-0.054	0.8	8.140
64	342.99	342.654	7.963	-0.059	0.8	8.138
65	344.00	344.122	7.963	-0.057	0.8	8.141
66	345.02	345.000	7.970	-0.059	0.8	8.143
67	345.98	345.619	7.954	-0.061	0.8	8.137
68	347.01	347.353	7.965	-0.070	0.8	8.141
69	348.03	348.143	7.971	-0.071	0.8	8.140
70	348.97	349.467	7.968	-0.078	0.8	8.143
71	349.94	350.078	7.945	-0.085	0.8	8.143
72	350.93	351.400	7.958	-0.091	0.8	8.144
73	351.93	352.021	7.939	-0.080	0.8	8.138
74	352.98	352.782	7.943	-0.079	0.8	8.139
75	354.08	354.804	7.945	-0.085	0.8	8.136
76	355.01	355.000	7.950	-0.083	0.8	8.139
77	355.96	356.083	7.964	-0.089	0.8	8.144
78	357.03	357.000	7.962	-0.097	0.8	8.141

Deutsche WindGuard
Wind Tunnel Services GmbH, Varel

Deutsche WindGuard

Seite 5
Page

1322749
D-K-15140-01-00
09/2013

Angegeben ist die erweiterte Messunsicherheit, die sich aus der Standardmessunsicherheit durch Multiplikation mit dem Erweiterungsfaktor k=2 ergibt. Sie wurde gemäß DAkkS-DKD-3 ermittelt. Der Wert der Messgröße liegt mit einer Wahrscheinlichkeit von 95 % im zugeordneten Wertintervall.

Die Deutsche Akkreditierungsstelle GmbH ist Unterzeichnerin der multilateralen Übereinkommen der European co-operation for Accreditation (EA) und der International Laboratory Accreditation Cooperation (ILAC) zur gegenseitigen Anerkennung der Kalibrierscheine. Die weiteren Unterzeichner innerhalb und außerhalb Europas sind den Internetseiten von EA (www.european-accreditation.org) und ILAC (www.ilac.org) zu entnehmen.

The expanded uncertainty assigned to the measurement results is obtained by multiplying the standard uncertainty by the coverage factor k = 2. It has been determined in accordance with DAkkS-DKD-3. The value of the measurand lies within the assigned range of values with a probability of 95%.

The DAkkS is signatory to the multilateral agree-ments of the European co-operation for Accredita-tion (EA) and of the International Laboratory Accreditation Cooperation (ILAC) for the mutual recognition of calibration certificates

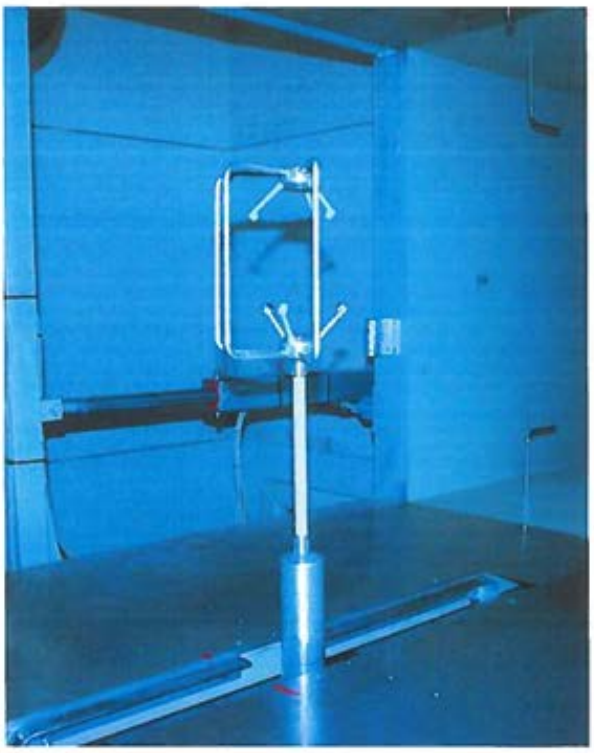

Image 1: Calibration set-up of flow direction test in the wind tunnel of Deutsche WindGuard, Varel. The sensor shown may differ from the calibrated one. Remark: The proportion of the set-up is not true to scale due to imaging geometry.

Deutsche WindGuard
Wind Tunnel Services GmbH, Varel

Deutsche WindGuard

Annex E. Table of calibration results

The results presented in the tables below are obtained by applying the same calibration procedure but with two different reference wind speed instruments, i.e. cup and sonic anemometers:

- Cup anemometer used for reference wind speed in:
  - Table 10: filtered 10-minute RWS data ("raw") ;
  - Table 11: binned RWS data ;
- Sonic anemometer used for reference wind speed in:
  - Table 12: filtered 10-minute RWS data ("raw") ;
  - Table 13: binned RWS data.

Table 12. Raw calibration results: 5-beam Demonstrator ; HWS measured by cup anemometer

	Azimuth sector ° / LOS	Range selected [m]	LOS dir [°]	Valid data points	Raw calibration					TI range	T abs 2m range
					"Free" regression			Forced regression			
					gain	offset	R2	gain	R2		
5-beam Avent lidar	0 (comb)	262	286,03	742	0,9980	0,0730	0,9992	1,0069	0,9991	10-17%	3-10°C
	1	252	285,99	502	1,0019	0,0510	0,9994	1,0077	0,9994	10-16%	2-7°C
	2	252	285,99	1087	1,0021	0,0562	0,9993	1,0091	0,9992	10-17%	4-8°C
	3	252	286,06	446	1,0092	0,0020	0,9992	1,0095	0,9992	9-16%	4-7.5°C
	4	252	285,99	1508	1,0034	0,0102	0,9991	1,0046	0,9991	10-18%	4-9°C
	0 (V1)	262	285,86	265	0,9920	0,1064	0,9990	1,0076	0,9987	11-17%	6-10°C
	0 (V2)	262	286,08	476	0,9975	0,0795	0,9991	1,0066	0,9990	11-17%	6-10°C

Table 13. Binned calibration results: 5-beam Demonstrator ; HWS measured by cup anemometer

	Azimuth sector ° / LOS	Range selected [m]	LOS dir [°]	Valid data points	Binned calibration					range of valid bins [m/s]		TI range	T abs 2m range
					"Free" regression			Forced regression					
					gain	offset	R2	gain	R2	min	max		
5-beam Avent lidar	0 (comb)	262	286,03	742	0,9982	0,0709	1,0000	1,0058	0,9999	4	13	10-17%	3-10°C
	1	252	285,99	502	1,0043	0,0314	1,0000	1,0072	0,9999	3,5	15,5	10-16%	2-7°C
	2	252	285,99	1087	1,0056	0,0267	1,0000	1,0084	1,0000	3	13,5	10-17%	4-8°C
	3	252	286,06	446	1,0097	-0,0046	0,9999	1,0090	0,9999	3,5	10	9-16%	4-7.5°C
	4	252	285,99	1508	1,0069	-0,0142	1,0000	1,0056	1,0000	3,5	15	10-18%	4-9°C
	0 (V1)	262	285,86	265	0,9943	0,0921	1,0000	1,0072	0,9998	4	9,5	11-17%	6-10°C
	0 (V2)	262	286,08	476	0,9973	0,0793	1,0000	1,0058	0,9999	4	13	11-17%	6-10°C

Table 14. Raw calibration results: 5-beam Demonstrator ; HWS measured by sonic anemometer

	Azimuth sector ° / LOS	Range selected [m]	LOS dir [°]	Valid data points	Raw calibration					TI range	T abs 2m range
					"Free" regression			Forced regression			
					gain	offset	R2	gain	R2		
5-beam Avent lidar	0 (comb)	262	286,86	745	0,9979	0,0307	0,9985	1,0017	0,9985	10-17%	3-10°C
	1	252	286,53	503	1,0024	0,0040	0,9989	1,0029	0,9994	10-16%	2-7°C
	2	252	287,02	1086	0,9931	0,0822	0,9988	1,0033	0,9987	10-17%	4-8°C
	3	252	286,83	445	0,9959	0,0521	0,9984	1,0033	0,9984	9-16%	4-7.5°C
	4	252	286,72	1508	0,9975	0,0148	0,9980	0,9992	0,9980	10-18%	4-9°C
	0 (V1)	262	286,68	267	0,9864	0,0804	0,9972	0,9981	0,9971	11-17%	6-10°C
	0 (V2)	262	286,85	477	0,9961	0,0613	0,9988	1,0031	0,9987	11-17%	6-10°C

Table 15. Binned calibration results: 5-beam Demonstrator ; HWS measured by sonic anemometer

	Azimuth sector ° / LOS	Range selected [m]	LOS dir [°]	Valid data points	Binned calibration					range of valid bins		TI range	T abs 2m range
					"Free" regression			Forced regression					
					gain	offset	R2	gain	R2	min	max		
5-beam Avent lidar	0 (comb)	262	286,86	745	1,0019	-0,0005	0,9999	1,0018	0,9999	3,5	13	10-17%	3-10°C
	1	252	286,53	503	1,0041	-0,0057	0,9999	1,0036	0,9999	3,5	15,5	10-16%	2-7°C
	2	252	287,02	1086	0,9990	0,0384	0,9999	1,0030	0,9999	3,5	13,5	10-17%	4-8°C
	3	252	286,83	445	0,9934	0,0613	0,9999	1,0018	0,9998	3,5	10	9-16%	4-7.5°C
	4	252	286,72	1508	1,0049	-0,0367	0,9999	1,0014	0,9999	3,5	15	10-18%	4-9°C
	0 (V1)	262	286,68	267	0,9878	0,0712	0,9999	0,9977	0,9998	4	9,5	11-17%	6-10°C
	0 (V2)	262	286,85	477	0,9957	0,0687	0,9999	1,0031	0,9999	4	13	11-17%	6-10°C

Annex F. Høvsøre wind rose

The wind climate in DTU's test section, Høvsøre, on the West coast of Jutland is the figure below.

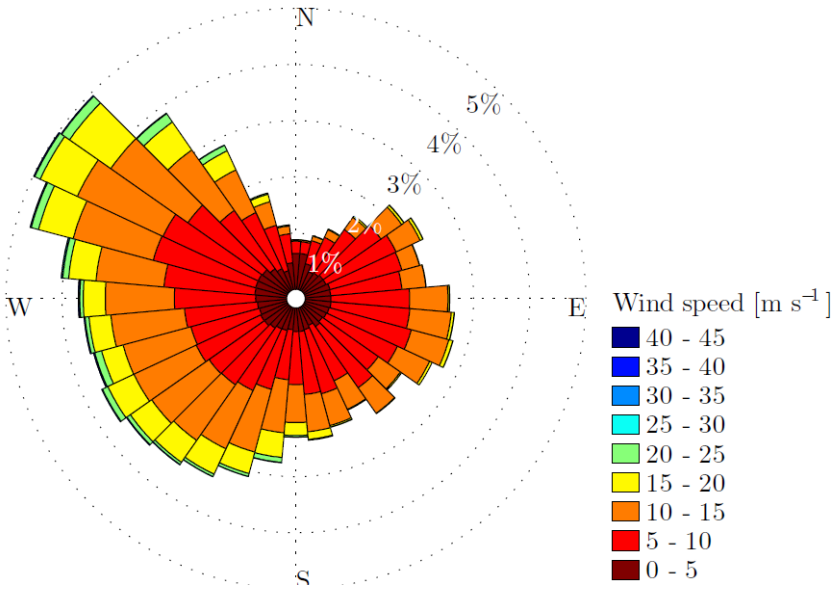

Figure 25. Wind rose at 100m in Høvsøre, between 2005-2013

(Reproduced with permission from A. Penã, extracted from [9])

Annex G. Sensitivy analysis of the RWS measurement error to external atmospheric parameters

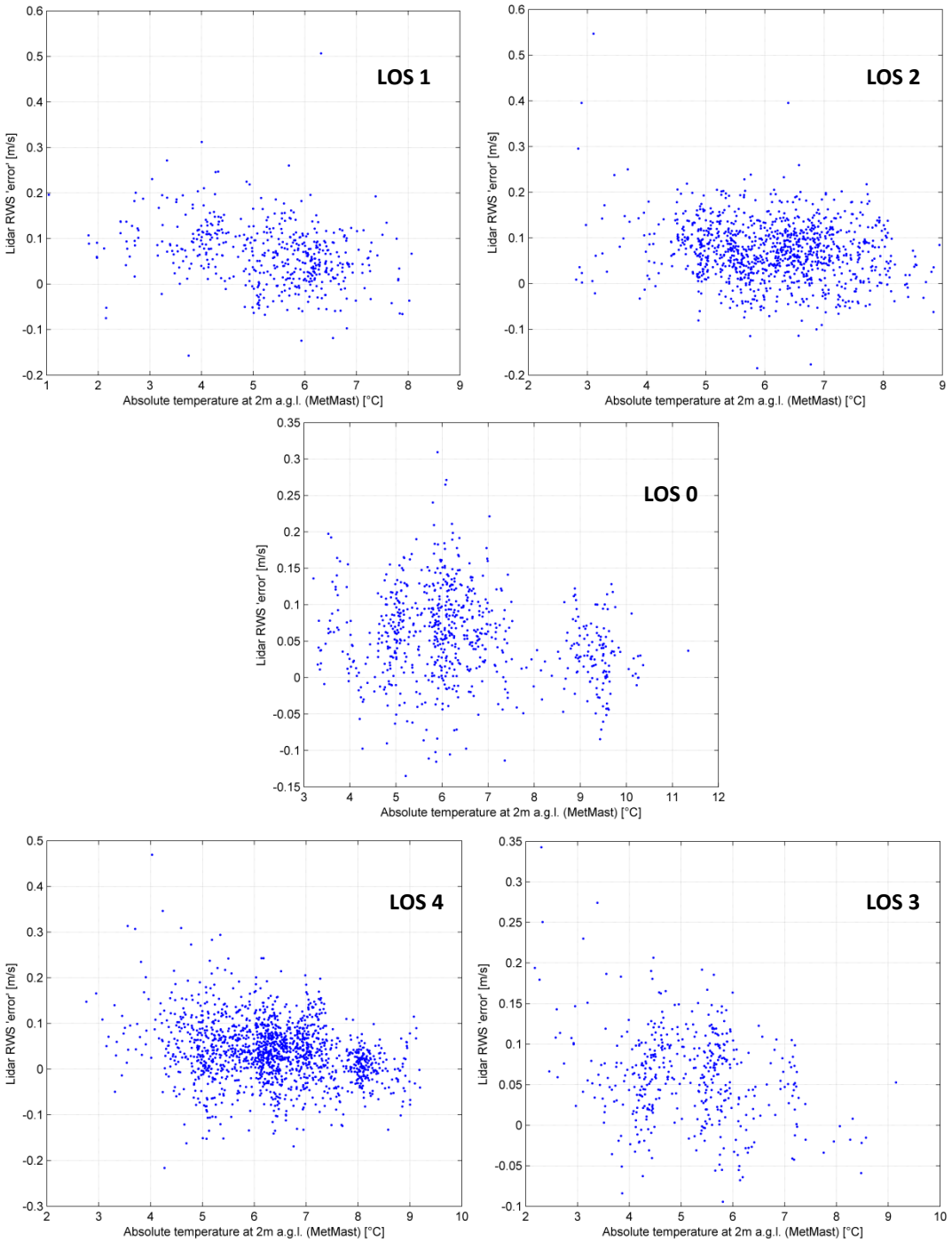

Figure 26. RWS measurement error vs. absolute temperature (at 2m a.g.l.) – all 5 beams

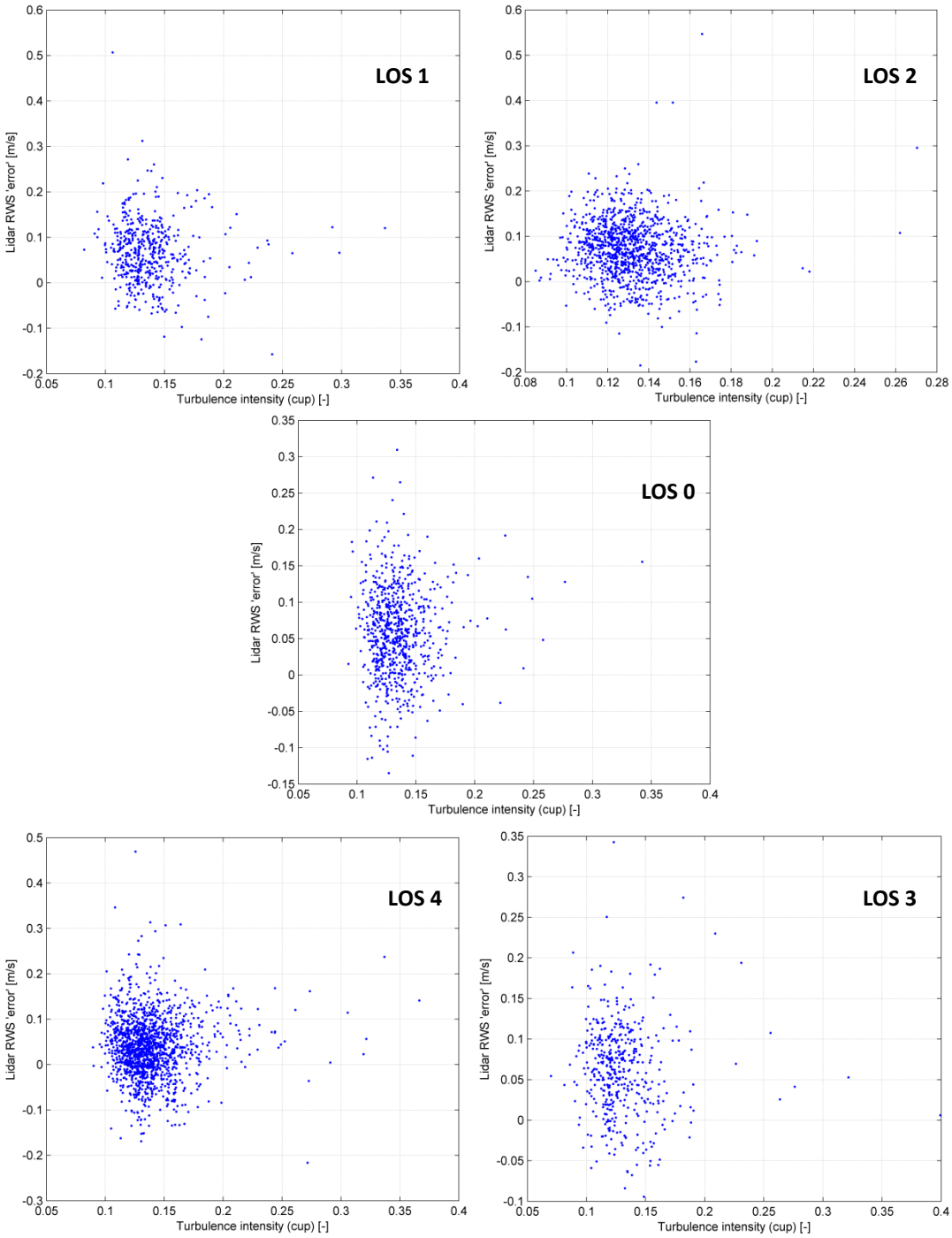

Figure 27. RWS measurement error vs. turbulence intensity – all 5 beams

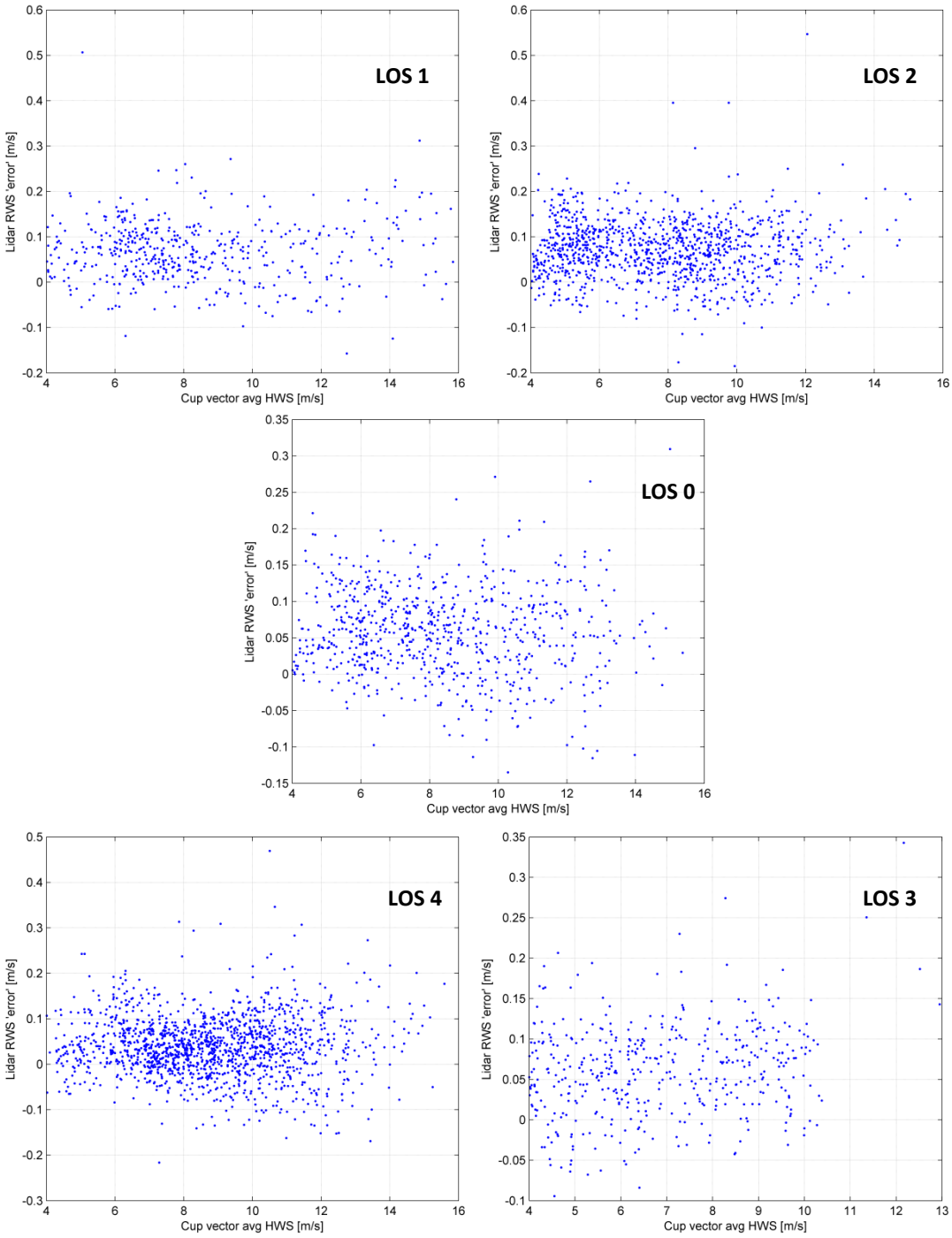

Figure 28. RWS measurement error vs. horizontal wind speed – all 5 beams

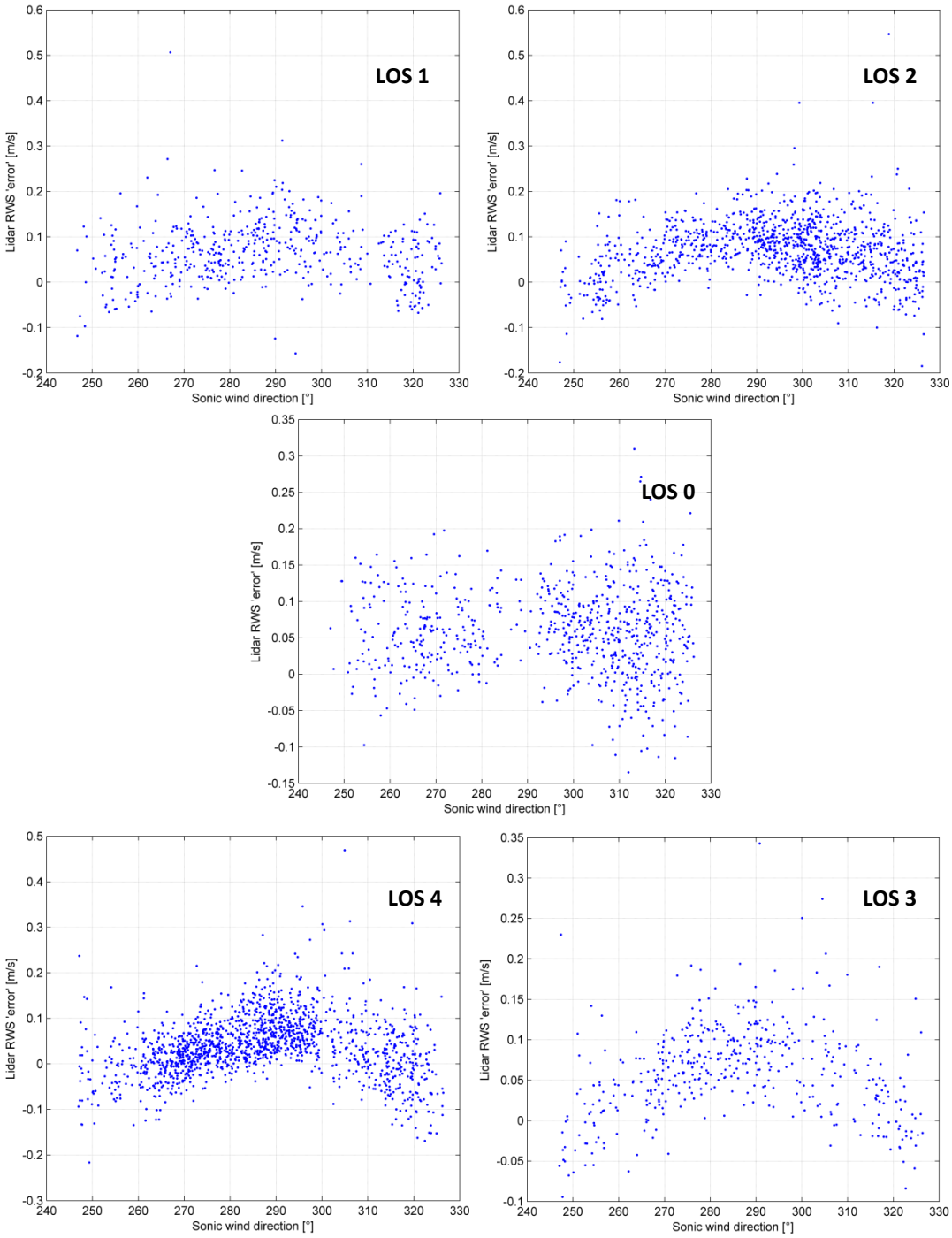

Figure 29. RWS measurement error vs. wind direction – all 5 beams

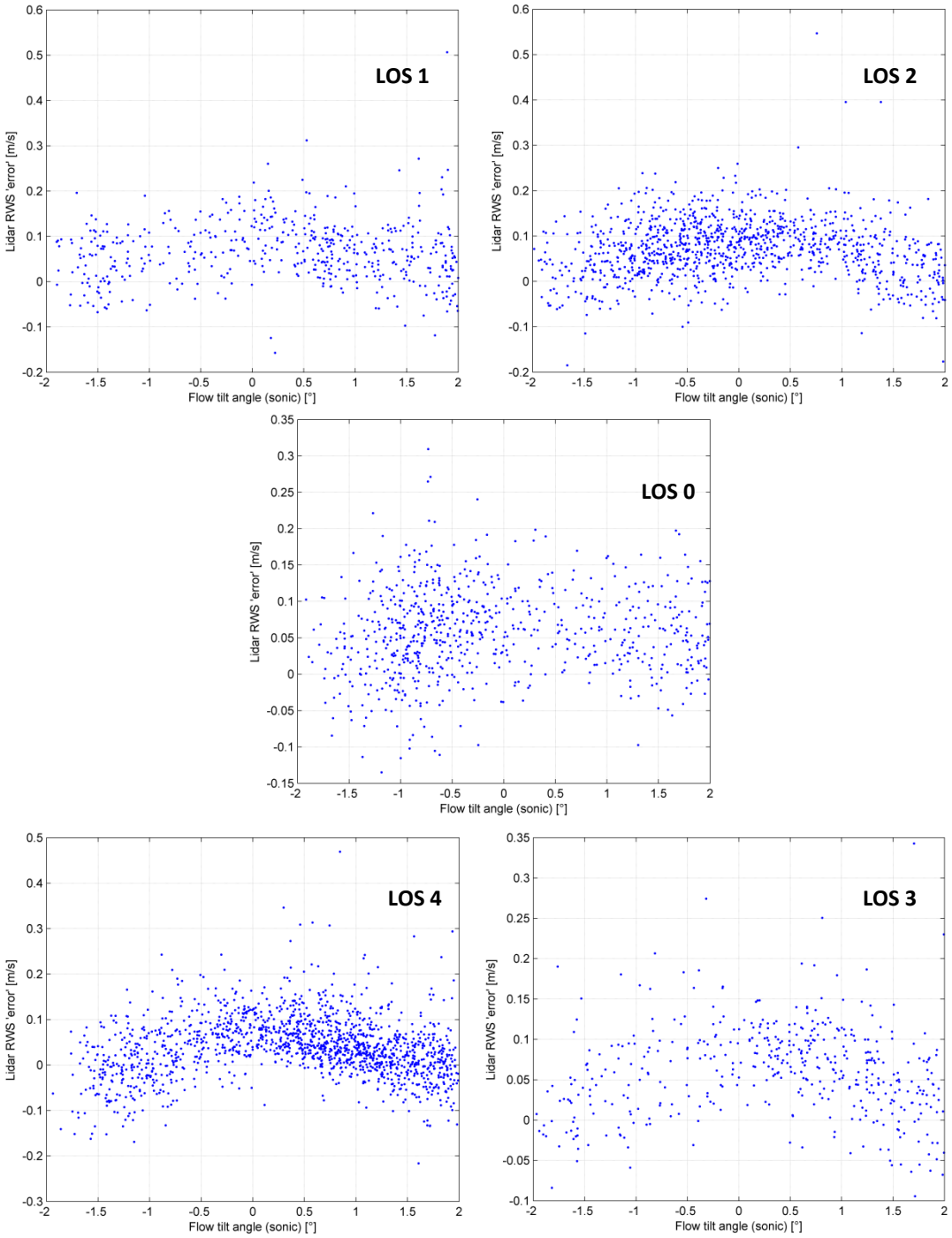

Figure 30. RWS measurement error vs. flow tilt angle – all 5 beams

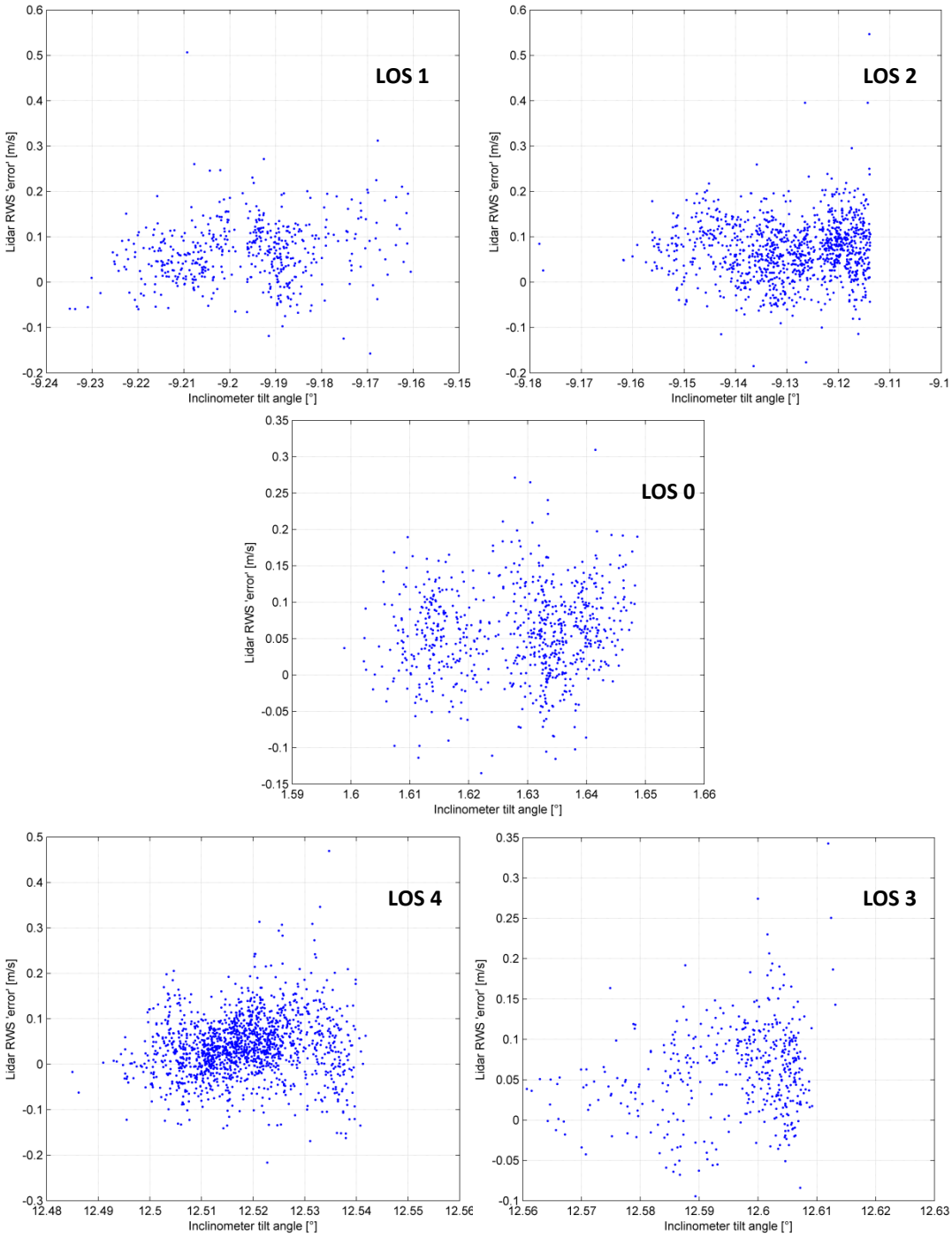

Figure 31. RWS measurement error vs. lidar tilt – all 5 beams

Annex H. Sensed range and timelag verification results – all 5 LOS

This annex provides the results of the sensed range and timelag verification results for all 5 LOS (see 3.5.2 for more information about the process).

For each figure, the graphs are:

- Top:
  - Left: sensed range vs. wind direction
  - Center: sensed timelag vs. wind direction
  - Right: maximum correlation coefficient vs. wind direction
- Bottom:
  - Left: sensed range vs. HWS
  - Center: sensed timelag vs. HWS
  - Right: maximum correlation coefficient vs. HWS

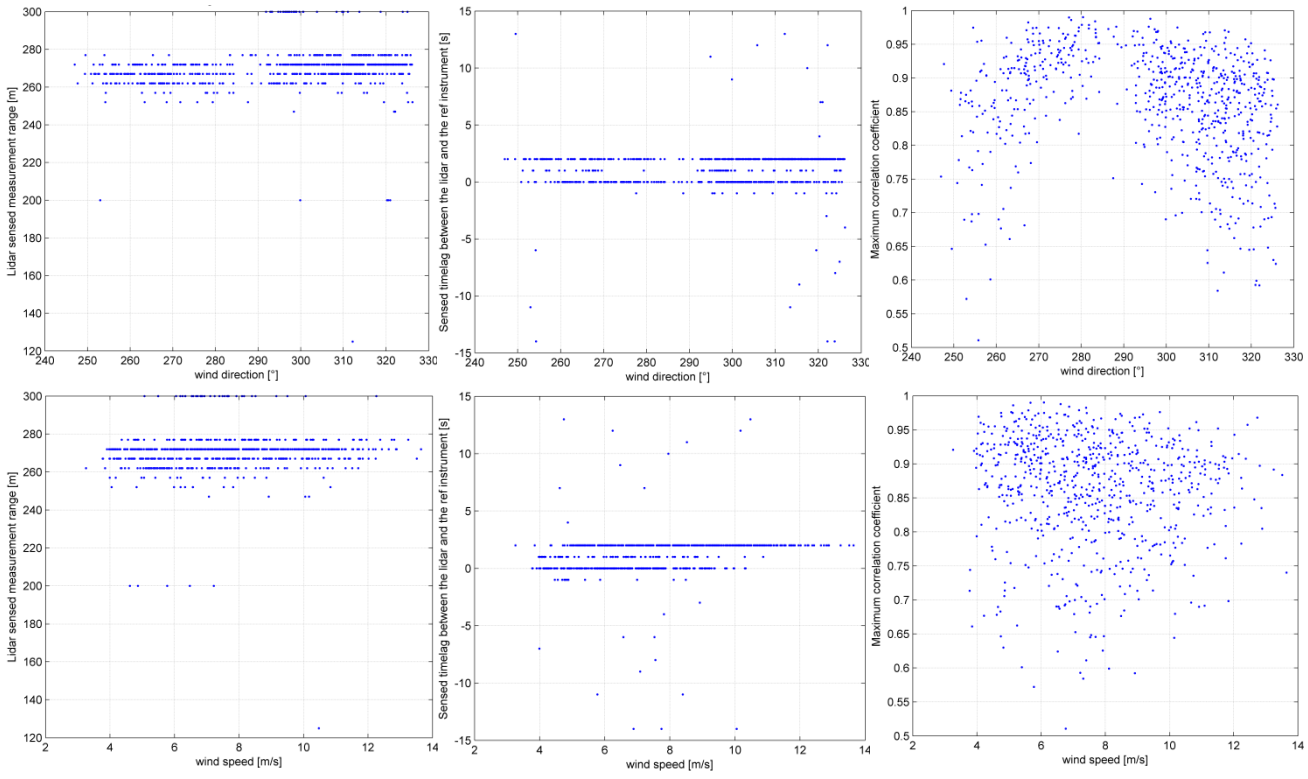

Figure 32. Sensed range and timelag verification for LOS 0

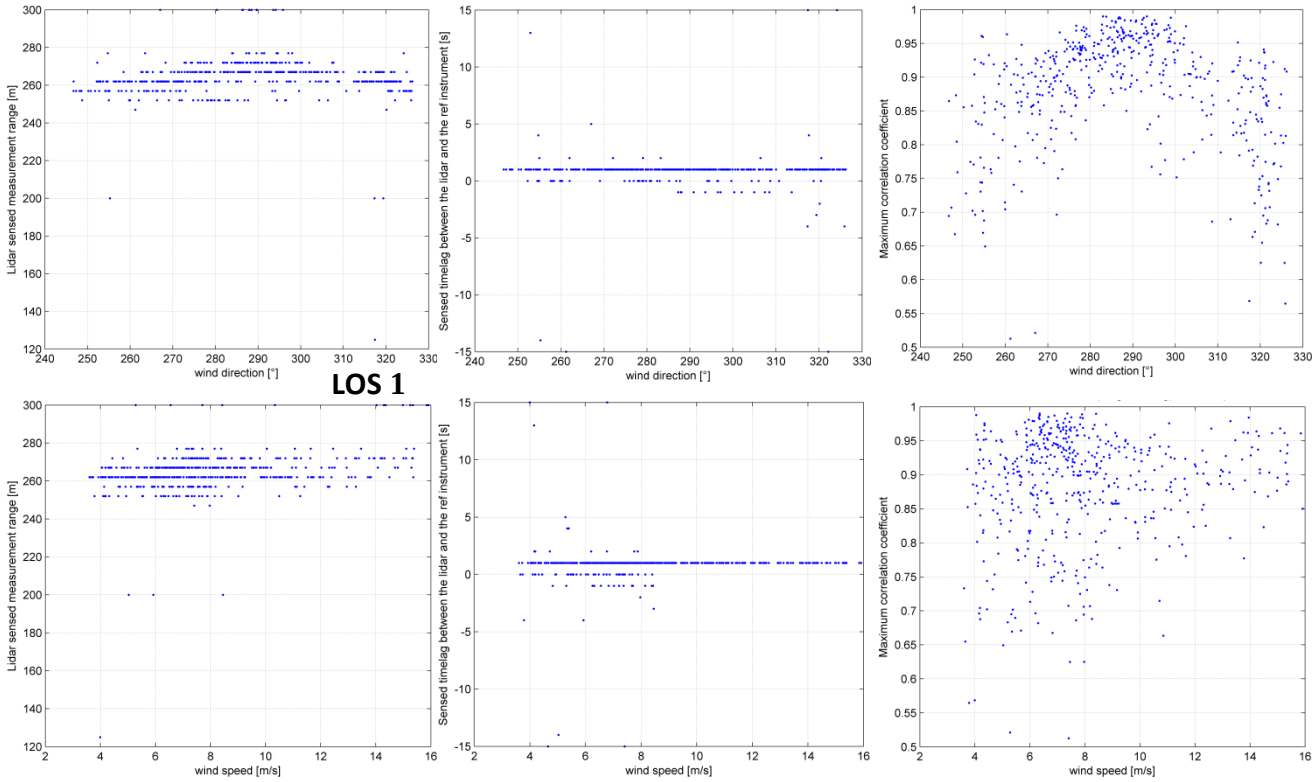

Figure 33. Sensed range and timelag verification for LOS 1

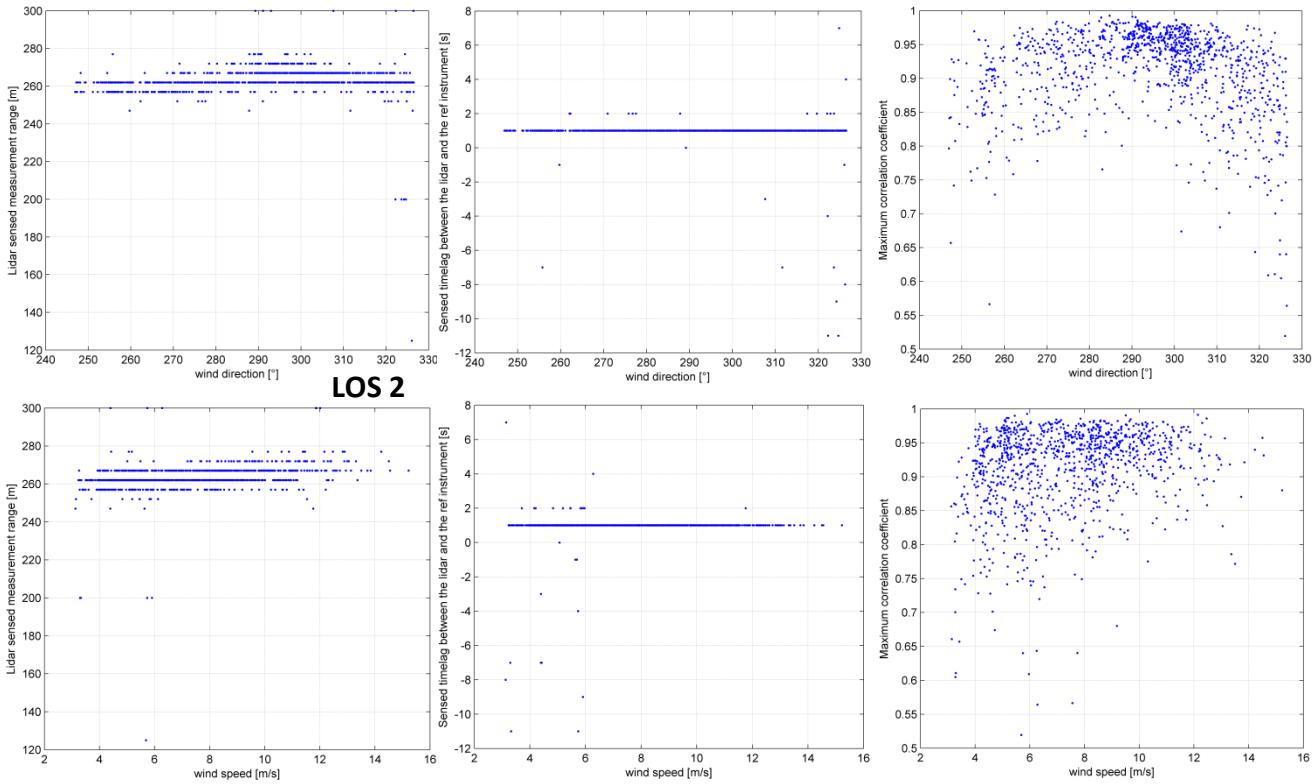

Figure 34. Sensed range and timelag verification for LOS 2

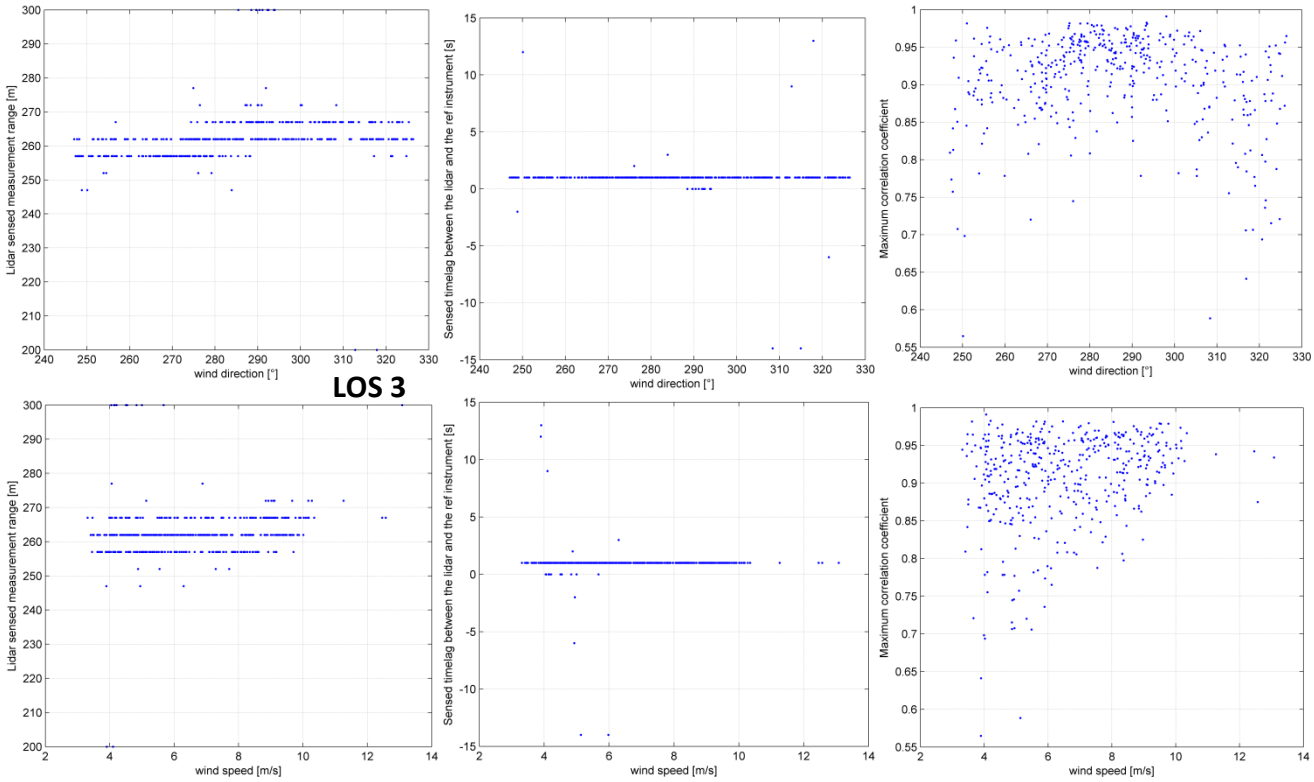

Figure 35. Sensed range and timelag verification for LOS 3

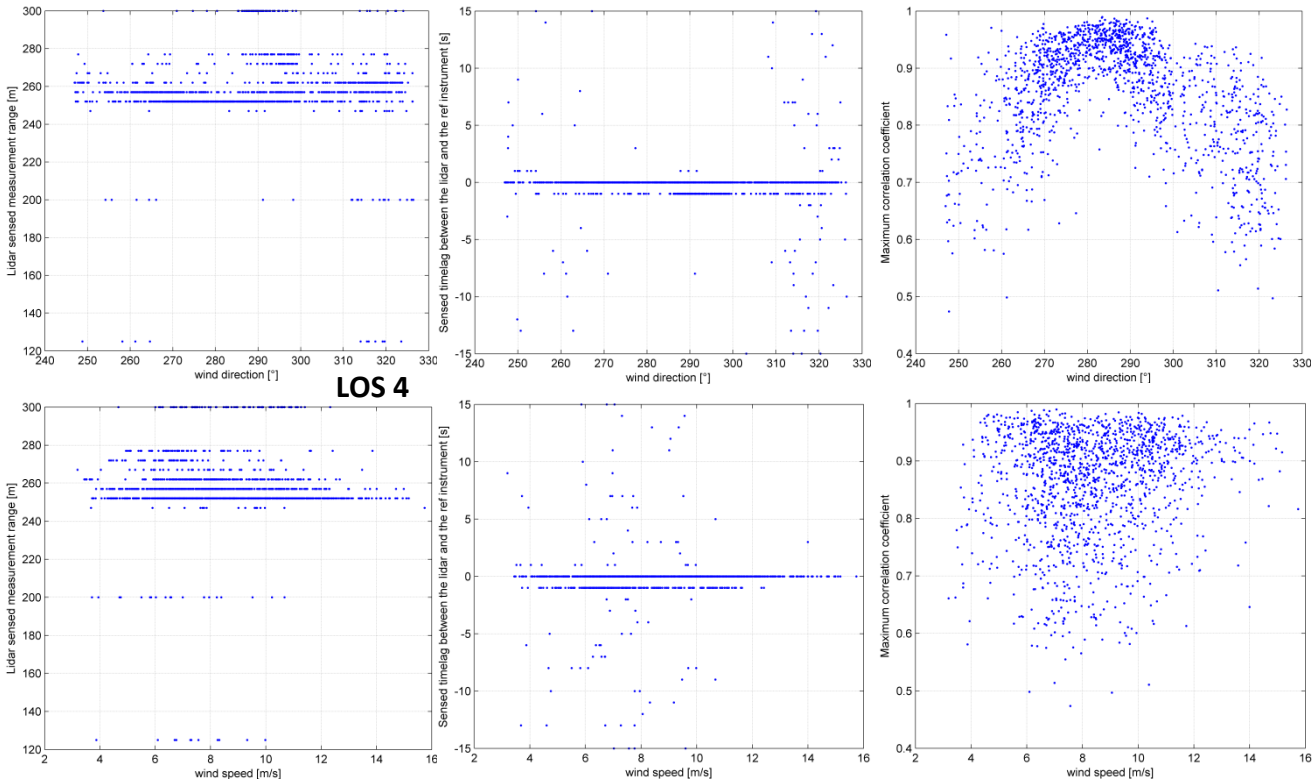

Figure 36. Sensed range and timelag verification for LOS 4

Annex I. RWS uncertainty results – all 5 LOS

This annex provides the results of the RWS uncertainty assessment for all 5 LOS (see 4.1).

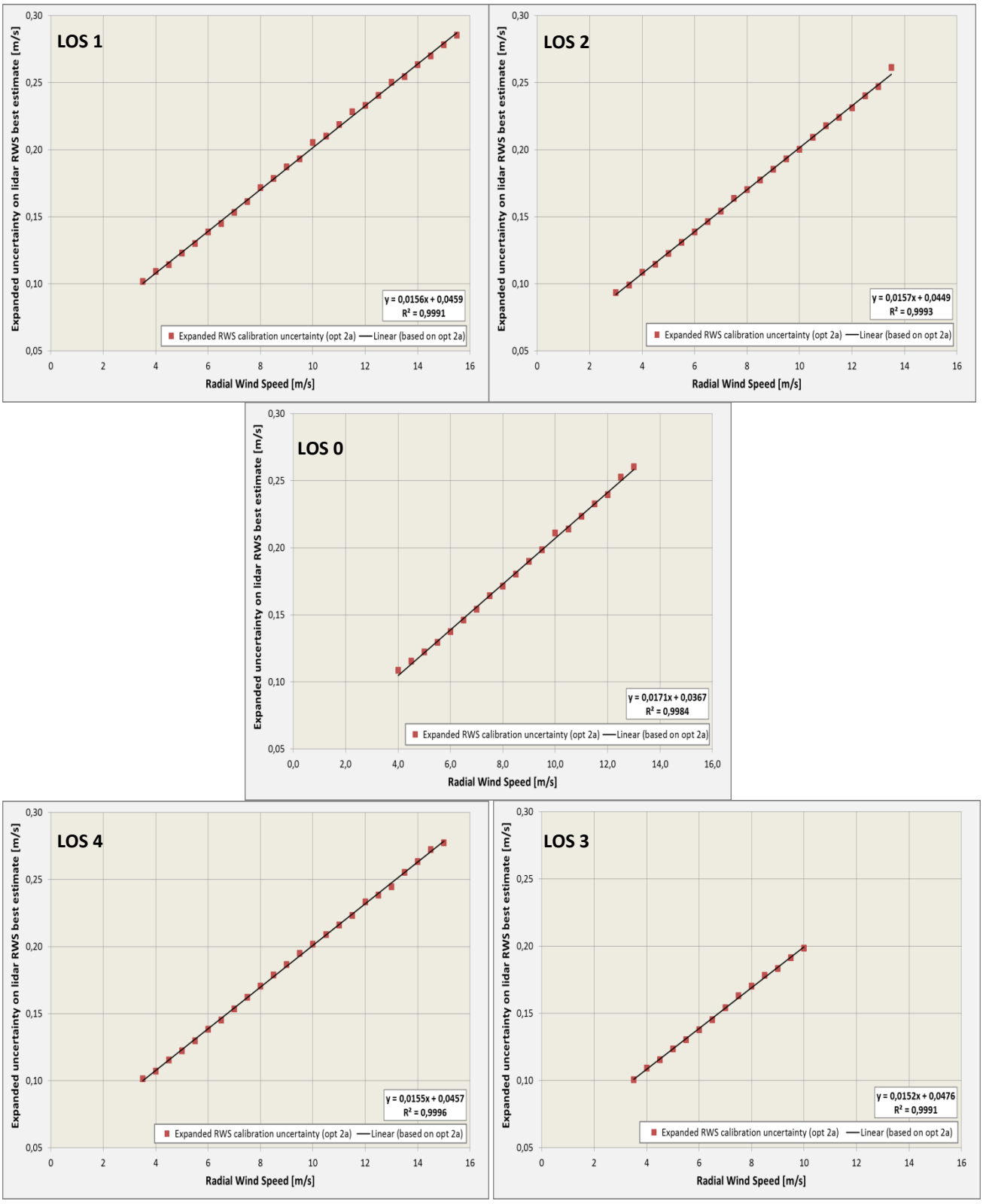

Figure 37. Expanded RWS uncertainty per bin – all 5 beams.

References

[1] Wagner R.: "Accounting for the speed shear in wind turbine power performance measurement", [2010], Risø-PhD-58(EN), ISSN: 1095-4244 (*http://dx.doi.org/10.1002/we.509*), vol: 14, issue: 8, pages: 993-1004, 2011.

[2] Wagner R., Pedersen T.F., Courtney M., Antoniou I., Davoust S., Rivera R.L.: "Power curve measurement with a nacelle mounted lidar", [2014], Wind Energy, Vol: 17, issue: 9, pages 1441–1453 (*http://dx.doi.org/10.1002/we.1643*).

[3] Borraccino A., Courtney M., Wagner R.: "Generic methodology for calibrating profiling nacelle lidars", [2015], DTU Wind Energy E-0086.

[4] Courtney M.: "Calibrating nacelle lidars", [2013], DTU Wind Energy E-0020(EN).

[5] JCGM 200:2012: "International Vocabulary of Metrology – Basic and General Concepts and Associated Terms" (VIM 3rd edition), (http://www.bipm.org/en/publications/guides/vim.html)

[6] JCGM 100:2008: "Evaluation of measurement data – Guide to the expression of uncertainty in measurement" (GUM), (http://www.bipm.org/en/publications/guides/)

[7] Westermann D., Rehfeldt K.: "Summary of cup anemometer classification" (for Thies First Class Advanced), Deutsche WindGuard GmbH (http://www.thiesclima.com/Anemometer%204.3351.%20classification%2012%202008%20.pdf)

[8] IEC 61400-12-1: Draft CDV, 30 April 2014, "Power performance measurements of electricity producing wind turbines"

[9] A. Penã et. Al: "Ten years of boundary-layer and wind-power meteorology at Høvsøre, Denmark" (*http://dx.doi.org/10.1007/*s10546-015-0079-8)